Details of the research work/project conducted by the Applicant to be described under the following headings: -

Title – Lipocalin 2 expression promotes tumor progression and therapy resistance by inhibiting ferroptosis in colorectal cancer.

Introduction

The first line of treatment in patients with colorectal cancer (CRC) is curative surgery (reviewed in [1]). In most cases, stage III and IV tumors are given adjuvant chemotherapy comprising 5-fluorouracil (5FU) and Oxaliplatin (reviewed in [1]). The standard of care for patients with locally advanced rectal cancer is neoadjuvant chemoradiotherapy (NACTRT), 45-50Gy of radiation over 5-6 weeks, and Capecitabine (an orally administered prodrug of 5FU) at a dose of 825mg/m^2 twice daily. Responders to NACTRT that are deemed operable undergo surgery, while the non-responders undergo further rounds of chemotherapy followed by surgery if the disease becomes operable[2]. However, a large number of patients relapse and develop drug resistant disease (reviewed in [1]) and while multiple mechanisms have been postulated to contribute to therapy resistance in CRC (reviewed in [3]), identifying markers that predict therapy response or targeted therapies that can overcome therapy resistance are not available in the clinic.

Ferroptosis is an iron dependent cell death mechanism that is distinct from other forms of cell death such as apoptosis and necroptosis (reviewed in [4]). The induction of ferroptosis is dependent on the presence of reactive iron radicals [5] and an inability to reduce peroxidated phospholipids either due to a decrease in the levels of the enzyme glutathione peroxidase (GPX4) [6, 7] or due to a decrease in glutathione (GSH) production due to a decrease in cystine import by the cystine glutamate transporter, system xC^-[8]. Consistent with these observations, compounds that inhibit the accumulation of lipid peroxides such as Liproxtatin [9] and ferrostatin [5] inhibit ferroptosis while compounds that inhibit the activity of GPX4 (RSL3) or system x_c^- (Erastin) [10-12] promote ferroptotic cell death. Notably, the inhibition of ferroptosis using either drugs or genetic manipulation [13, 14] confers chemo-resistance in cancer cells suggesting that this pathway could serve as an important target in tumors that are resistant to cytotoxic therapeutics.

Lipocalin2 (LCN2), also known as NGAL (neutrophil gelatinase associated lipocalin), is a secreted glycoprotein [15, 16] and is required to maintain the integrity of the gastro-intestinal mucosa [17]. LCN2 forms a complex with bacterial and human siderophores (reviewed in [15]) thereby regulating iron homeostasis in cells. Iron-bound LCN2 is imported into cells by complex formation with the LCN2 receptors, SLC22A17, MCR4, and LRP2[15, 18]. LCN2 binds to and protects the matrix-metalloprotease MMP9 from auto-degradation with a concomitant increase in MMP9 activity LCN2 is over-expressed in many tumour types (reviewed in [15, 19]), including colorectal cancer[15, 19], and is an indicator of colon cancer progression from adenoma to carcinoma[20-22]. LCN2 over-expression leads to increased tumor formation in xenograft models of colon cancer[21]. LCN2 also provides resistance against serum starvation, UV irradiation, and cisplatin [23]. Further, an increase in LCN2 levels leads to resistance against X-ray irradiation in oral cancer and lung cancer [24]. Other reports suggest that LCN2 expression is increased in breast cancer [25-27] and loss of LCN2 expression leads to decreased tumour progression in mouse models of human breast cancer [28, 29]. In addition, agents that inhibit LCN2 expression can inhibit transformation and neoplastic progression in breast cancer cell lines in culture[30, 31]. Further, LCN2 expression is associated with angiogenesis in both breast and pancreatic cancer [32, 33] and inhibition of LCN2 expression with siRNA inhibits angiogenesis [30]. However, there is very little evidence that correlates LCN2 levels with the response to radio or chemotherapy or evidence to suggest that inhibiting LCN2 expression with a therapeutic agent could lead to tumour regression. Therefore, a molecule that can inhibit LCN2 mediated tumour progression and resistance to chemo and radiotherapy could serve as a potent therapeutic agent in multiple tumour types.

We previously demonstrated that LCN2 is required to increase invasion and tumor progression observed upon plakophilin3 (PKP3) loss in the colon cancer cell line HCT116[34]. This report indicates that LCN2 levels correspond with an increase in resistance to 5-fluorouracil (5FU). The resistance is dependent on the ability of LCN2 to inhibit ferroptosis by sequestering iron and stimulating the expression of *xCT* and *GPX4*. Finally, inhibiting LCN2 function with a monoclonal antibody sensitizes cells to therapy and inhibits tumor growth in xenograft mouse models.

Objectives:

1) To determine the levels of LCN2 in different colon cancer cell line models and colon cancer patient samples.
2) To determine the mechanism by which LCN2 leads to increase in 5 FU resistance.
3) To develop monoclonal antibody against LCN2
4) To determine whether inhibition of LCN2 function with LCN2 antibody leads to tumor regression and therapy sensitivity.

Material and Methods:

Patient Samples: Tumor samples of 80 colon cancer patients were obtained from the ACTREC and TMH tissue repositories. A pathologist analyzed hematoxylin and Eosin-stained slides to confirm the presence of normal and tumor tissue.

Plasmids and constructs: The oligonucleotides used to generate the LCN2, xCT, and ETS1 shRNA constructs (Table1) were cloned downstream of the U6 promoter in pLKO.1hygro and pLKO.1puro respectively.

Name of gene	Sequence (5' to 3')
shRNA LCN2.X Forward	CCGGAAGATGTATGCCACCATCTATCTCGAGATAGATG GTGGCATACATCTTTTTTTG
shRNA LCN2.X Reverse	AATTCAAAAAAAGATGTATGCCACCATCTATCTCGAGA TAGATGGTGGCATACATCTT
shRNA LCN2.Y Forward	CCGGAACTACAACCAGCATGCTATGCTCGAGCATAGCA TGCTGGTTGTAGTTTTTTTG
shRNA LCN2.Y Reverse	AATTCAAAAAAACTACAACCAGCATGCTATGCTCGAGC ATAGCATGCTGGTTGTAGTT
shRNA XCT Forward	CCGGGCTGAATTGGGAACAACTATACTCGAGTATAGTT GTTCCCAATTCAGCTTTTTG
shRNA XCT Reverse	AATTCAAAAAGCTGAATTGGGAACAACTATACTCGAGT ATAGTTGTTCCCAATTCAGC
shRNA ETS1 Forward	CCGGCTGGAATTACTCACTGATAAACTCGAGTTTATCAG TGAGTAATTCCAGTTTTTG
shRNA ETS1 Reverse	AATTCAAAAACTGGAATTACTCACTGATAAACTCGAGT TTATCAGTGAGTAATTCCAG

Table 1. Sequences of oligonucleotides used to generate shRNA constructs.

Cell lines and transfections: HCT 116 cells (RRID: CVCL_0291) were obtained from Dr. Bert Vogelstein, HT-29 (RRID: CVCL_0320), and DLD-1 (RRID: CVCL_0248) were

obtained from Dr. Sanjeev Galande. Cell line authentication was performed using short tandem repeat profiling within the last three years and cultured as described [34-36]. All experiments were performed with mycoplasma-free cells. All cell lines were cultured at 37 °C in a humidified atmosphere with 5% CO_2 in culture medium supplemented with 10% fetal bovine serum (FBS) and 1% penicillin-streptomycin. HCT116 and HT29 were cultured in DMEM, and DLD1 was cultured in RPM11640. The HCT116 derived vector control clone (vec), PKP3 knockdown clones (shpkp3-1 and shpkp3-2), the LCN2+PKP3 double knockdown clones (shpkp3-2+shlcn2-1 andshpkp3-2+shlcn2-3) and the shpkp3-2 derived vector control clone (shpkp3-2-vec) cells were cultured as previously described (77, 78). The HCT116 derived LCN2 overexpressing cell lines (LCN2.1 and LCN2.3) and the vector control (PTPCD1) were generated by transfecting the HCT116 cell line with the pCDNA3.1 vector expressing LCN2 or pCDNA31, respectively using Lipofectamine LTX reagent (Life Technologies) as per the manufacturer's instructions. The cells were maintained in media containing 500µg/ml G418 to obtain single-cell clones. The xCT knockdown stable cell lines were generated by transfecting the PKP3 knockdown clone, shpkp3-2, DLD1, and HT29 cell lines with the pLKO.1 EGFP-f-puro vector expressing an shRNA targeting xCT using Lipofectamine LTX reagent (Life Technologies) or the empty vector to generate the vector controls. The cells were maintained in media containing 0.5µg/ml puromycin to obtain single-cell clones. Lipofectamine LTX reagent (Life Technologies) was also used for transient transfection of the plKO.1 hygro vector expressing the shRNA targeting ETS1 in PKP3 knockdown clone shpkp3-2 and HT29 cell line.

Chemicals: N-Acetyl-L-Cysteine (catalogue number A-7250, Sigma), Erastin (catalogue number E-7781, Sigma), RSL3 (catalogue number SML2234, Merck), Liproxtatin (catalogue number SML-1414, Sigma), ferrostatin (catalogue number SML-0583, Sigma), Z-VADFMK (catalogue number SC-3067, Sigma), Necrostatin (catalogue number CAS 4311-88-0, Sigma) and Catechol (catalogue number C-9510, Sigma).

Clonogenic survival assays: 10^3 cells were seeded in 35mm cell culture plates and allowed to attach overnight. Cells were either pre-treated with the vehicle control or 5FU or the vehicle control or 5FU in combination with other compounds (NAC, Ferrostatin, Necrostatin, Liproxtatin, Z-VAD-FMK, RSL3, and Erastin) for 48 hours. Similarly, cells treated with the vehicle control or 5FU were incubated with antibodies (3D12B2 and mIgG) or recombinant LCN2 proteins. The media was changed after 48 hours post-treatment, and fresh media supplemented with 10% FBS was added. After incubation for 14 days, colonies were fixed using 4% paraformaldehyde. The cells were then stained with 1% crystal violet for 1 hour. The number of colonies was counted and used to generate the survival curves for each clone. The

survival curves were plotted using the values obtained for the survival fraction on the Y-axis (log scale) and the corresponding treatment on the X-axis where: Survival fraction (SF) = (number of colonies formed after treatment)/ (number of colonies seeded x Plating efficiency) In this equation Plating efficiency (PE) = number of colonies formed from untreated cells/ number of untreated cells seeded.

Soft Agar Assays: Soft agar colony formation assays were performed in triplicate as described [34]. The results shown are an average of three independent experiments

Isolation of total RNA and real-time PCR reactions: The forward and reverse oligonucleotides used in this study are shown in Table2. Quantitative reverse transcriptase PCRs were performed as described[34], and GAPDH levels were used for normalization in all experiments.

Name of gene	**Sequence (5' to 3')**
GAPDH Forward	TGCACCACCAACTGCTTAGC
GAPDH Reverse	GGCATGGACTGTGGTCATGAG
LCN2 Forward	CCTCTACGGGAGAACCAAGGAGC
LCN2 Reverse	ACCTGTGCACTCAGCCGTCG
ETS1 Forward	GGCAGTTTCTTCTGGAATTA
ETS1 Reverse	CACGGCTCAGTTTCTCATA
mxCT F	GAGGACAGGCTTTTGATTGCAG
mxCT R	AGGTAGGAGCTGGTCAACAGCA
XCT F	GCTCTTCGTGGCTCTGGGCAT
XCT R	TGGCATTGGGAGGCTGCT

Table 2. Sequences of Oligonucleotides used for quantitative RT-PCR. m indicates murine xCT.

Antibodies and Western blot analysis. Protein extracts were prepared either in EBC lysis buffer (120mM NaCl, 50mM Tris-HCL (pH 8), 0.5% NP40 and protease inhibitors [5µg/ml Leupeptin, 10 µg/ml Aprotinin, 0.2mM sodium orthovanadate and 100mM sodium fluoride])[37] or in 1X sample buffer as described[38]. Acetone precipitation of cell supernatants and Western blots were performed as described[34]. Antibody dilutions are shown in Table 3. The blots were developed using Super signal West Pico Chemiluminescent Substrate (Pierce), Super Signal West Femto Chemiluminescent Substrate (Pierce), and Clarity Western ECL substrate (Bio-Rad) as per the manufacturer's instructions.

Protein	Source	Type	Catalogue number	Company	Antibody dilution
β actin	Mouse	Monoclonal	A5316	Sigma	1:5000
PKP3	Mouse	Monoclonal	35-7600	Invitrogen	1:2000
LCN2	Goat	Polyclonal	AF1757	R&D Systems	1:2000
XCT	Rabbit	Monoclonal	12691	Cell Signalling	1:1000
GPX4	Rabbit	Monoclonal	Ab 125066	Abcam	1:1000
ETS1	Rabbit	Monoclonal	14069	Cell Signalling	1:1000
α tubulin	Rabbit	Monoclonal	Ab 52866	Abcam	1:1000
Anti-Mouse HRP	Goat	Secondary	A28177	Life Technologies	1:2500
Anti-Rabbit HRP	Goat	Secondary	G-21234	Life Technologies	1:5000
Anti-Goat HRP	Donkey	Secondary	sc2020	Santa Cruz	1:250

Table 3. The catalogue number, company name, and dilutions of antibodies used for Western blotting.

Total ROS detection using CellROX™ or DCFDA: Oxidative stress was detected by the fluorogenic CellROX™® orange kit (Thermo Fisher Scientific, Inc.) or a DCFDA Cellular ROS Detection Assay Kit, Abcam (ab113851) as per the manufacturer's instructions. Briefly, $2x10^3$ cells were seeded into in CoStar® 96 well- black with clear flat bottom plate. Cells were allowed to attach and then treated with 5FU and incubated for the indicated times. Cells were then incubated for 45 min at 37 °C in the dark in the presence of 5 µM CellROX™ or 25 µM DCFDA diluted in serum-free adhesion medium without phenol red according to the manufacturer's instructions. Fluorescence intensity was measured in a fluorescence microplate reader at 535 nm excitation and 565 nm emission wavelengths for CellROX™® and 485 nm excitation and 535 nm emission wavelengths for DCFDA.

Lipid ROS detection using BODIPY C11: BODIPY C11 was used for the detection of lipid ROS. Briefly, $2x10^3$ cells were seeded into in costar® 96 well- Black with Clear Flat Bottom plate. Cells were allowed to attach overnight and then treated with 5FU for the indicated time. Cells were then treated with 10 µM of BODIPY and incubated for 30 minutes at 37°C in a 5% CO_2-humidified atmosphere. The fluorescence was recorded at separate wavelengths, one at excitation/emission of 581/591 nm for the reduced dye and the other at

excitation/emission of 488/510 nm for the oxidized dye. The ratio of the emission fluorescence intensities at 590 nm to 510 nm gives the read-out for lipid peroxidation in cells.

Detection of Ferric and Ferrous iron: Ferric and ferrous iron were detected in the cells using an iron assay kit (Abcam) as per the manufacturer's instructions.

Determination of GSH levels: GSH levels were determined by Promega GSH-Glo™ Glutathione Assay kit as per the manufacturer's instruction. Briefly, 4000 cells were seeded in costar® 96 well- Black with Clear Flat Bottom plate and allowed to attach overnight. Media was removed, and 100 ul of GSH-Glo™ reagent was then added to each well and allowed to incubate at RT for 30 minutes. After incubation 100 µl of reconstituted Luciferin Detection Reagent was added to each well, and luminescence measured after a 15-minute incubation**.**

Chromatin Immunoprecipitation: Cells were washed with 1X PBS followed by fixation with 1% (v/v) formaldehyde for 10 min at RT and quenched with 0.25 M glycine. Further, cells were lysed and subjected to sonication for size selection (200-600 bp DNA fragment). 5% input served as a control, and the rest of the lysate was equally divided and used for immunoprecipitation with either non-specific IgG or the ETS1 antibody. The DNA was eluted for ChIP-qPCR. The percent input was then determined related to input DNA.

Name of gene	**Sequence (5' to 3')**
xCT promoter Forward	GCTGTAGTAAGTTGGTGTGACAGG
xCT promoter Reverse	GCTGCCGCCCTATCATTACAAACC
LCN2 promoter Forward	TCCTGACCAGGTGCAGAA
LCN2 promoter Reverse	GGTGGCCCTATTTATGGGATCT

Table 4. Sequences of Oligonucleotides used for ChIP.

Determination of Catechol levels by LC-MS/MS ESI Q-TRAP:

An MRM (Multiple Reaction Monitoring) method in negative mode was developed for the determination of simple Catechol with LC/MS-MS-ESI QTRAP instrument using standard Catechol (C6H6O2) (Molecular weight 110.1 g/mol) of purity 99.99% ordered from Sigma Aldrich. Various concentrations of catechol, ranging from (3.1 ng/ml to 100 ng/ml) were prepared in methanol: water (50:50 v/v) for calibration.

Methanol - LC-MS/MS Grade (Sigma Aldrich), Water – MilliQ (Millipore), 100mM Dipotassium phosphate (K2HPO4) (pH 11.5)- Extra pure (Merck), Formic Acid - LC-MS/MS Grade (Sigma Aldrich), Acetonitrile - LC-MS/MS Grade (Sigma Aldrich), Pyrocatechol (C6H6O2)-99.99% purity (Sigma Aldrich)

MS/MS Fragment used to identify Catechol

Compound	Precursor Ion	MS/MS Fragment mass	Formula
Catechol	109.000	91.000	C6H6O2

Extraction and purification of catechol from the cells using a C18-E STRATA cartridge with a capacity of 50mg (obtained from Phenomenex®) and 100mM of K2HPO4 (pH 11.5), as per manufacturer's protocol. This protocol was designed considering few properties of catechol, such as its pKa value, molecular weight, degree of unsaturation, etc.

Cells were washed 2-3x with sterile distilled water to remove any residual media. The cells were collected in sterile Milli-Q water and placed on ice. Cells were mechanically disaggregated to make a single-cell suspension by passing them through a syringe 3-4 times and counted with a hemocytometer. 2x 10^6 cells were sonicated (8 cycles of 10 seconds each), and the lysate centrifuged and the pellet discarded.

A C18-E STRATSA cartridge with a capacity of 50mg (Phenomenex, Torrance, CA, US) was placed on a vacuum solid-phase extraction manifold. The cartridge was first conditioned with 1 ml of 100% methanol and then equilibrated with 1ml of 100mM Dipotassium Phosphate (K2HPO4) of pH 11.5, per the manufacturer's protocol. Subsequently, 1ml of cell lysate was loaded onto the SPE cartridge and drawn through by gravity. The cartridge was washed with 1ml of 100mM K2HPO4 of pH 11.5, followed by a wash with 1ml of 100% methanol. The flow-through obtained was discarded. Then, the sample was eluted into a new tube using 1ml of Formic acid: methanol (5:95 v/v)

The eluted sample was vacuum dried at 37ºC in Speed Vac evaporator and reconstituted in ~50µl of Acetonitrile: Methanol: Water (10:20:70 v/v/v) mix. The mixture was centrifuged to remove any debris, and the supernatant vacuum dried and reconstituted in 20µl of Acetonitrile: Methanol: Water (10:20:70v/v/v) mix. 15µl of this supernatant was taken in HPLC glass vials and used for further LC/MS-MS analysis.

Liquid chromatography was performed on a Shimadzu Nexera-X2 series equipped with a gradient pump with a vacuum degasser, an autosampler, and a column oven. The chromatographic separation was accomplished by Gradient mode elution. The mobile phase used was - Solvent A - 0.1% formic acid in water and solvent B–Acetonitrile with 0.1% formic acid in ACN. Mass spectrometric analysis was performed on a Triple Quadrupole LC/MS-MS QTRAP 4500 series mass spectrometer (AB SCIEX QTRAP 4500Canada) equipped with an Electro Spray Ionization (ESI) source. MS analysis was performed in the targeted multiple

reactions monitoring (MRM) negative mode. Data acquisition and processing were conducted using Analyst1.6.2 software.

Tumor formation in nude mice: 6-8 weeks old CD1 Nude mice (Crl: CD1-*Foxn1*^{nu}) provided by the ACTREC laboratory animal house facility were used for the study. Immunocompromised mice were injected subcutaneously in the dorsal flank with 1 X 10^6 cells of the HCT116 derived vector control (vec) or PKP3 knockdown clone (shpkp3-2) or 1 x 10^7 DLD1 cells. Once the DLD1 tumors grew, the mice were sacrificed, and 3mm^3 tumor pieces were transplanted into NOD SCID (NOD.CB17-Prkdcscid/NCrCrl) mice. Tumor formation and volume were monitored. Once the tumors reached a specific size (about 50-100 mm^3), the mice were either injected with the vehicle control (PBS) or 30 mg/kg 5-FU (IP) thrice a week for 2 weeks. Where indicated, 100µg of mouse IgG or 3D12B2 were injected IV every week. Tumor volume was determined using vernier calipers using the formula (0.5 X LV^2), where L is the largest dimension and V is the perpendicular dimension. The mean tumor volume and SEM are plotted on Y-axis, and the number of days is plotted on X-axis. p values were obtained using the student's t-test.

Antibody generation: Codon optimized_full-length LCN2 cDNA (NM_005564) was synthesized by Gene script and cloned into pET-28b (+) digested with NdeI and XhoI. LCN2 protein was expressed in and purified from *E.coli* Rosetta strain. BALB/c mice were injected with 10µg of pure protein with Freund's complete adjuvant in 1:1 ratio for primary immunization, followed by two boosters at a gap of 21 days each with Freund's Incomplete Adjuvant in 1:1 ratio. Before hybridoma production, a final injection of 50µg of protein in sterile 1X PBS (5x of the primary immunization) was given intraperitoneally. For hybridoma generation, splenocytes from the immunized mice were fused with mouse myeloma cells Sp2/O with the help of PEG (Poly-ethylene-glycol) in a ratio of 7:1. Thus, Hybridoma colonies were established using the HAT (hypoxanthine-aminopterin-thymidine)-HT (Hypoxanthine-Thymidine) selection method followed by ELISA to check antibody production Antibody producing colonies were single-cell cloned, amplified and the monoclonal antibody was purified from cell supernatant using Protein A beads.

Analysis of TCGA data: RNAseq gene expression, normalized (Log2X+1) counts for TCGA colon adenocarcinoma (PanCancer Atlas) were obtained from UCSC xena (https://xenabrowser.net/datapages/?dataset=TCGA.COAD.sampleMap%2FHiSeqV2&host=https%3A%2F%2Ftcga.xenahubs.net&removeHub=http%3A%2F%2F127.0.0.1%3A7222).

As per TCGA bar code, normal and tumor samples were distributed, and R 3.3.3 software

(http://www.R-project.org/) was used for box plot representation. p-value was calculated using the Wilcoxon-Mann- Whitney test analysis.

Pearson's correlation analysis: Colorectal adenocarcinoma (TCGA, firehose legacy (provisional data)) cohort was selected from cBioPortal, and mRNA expression z-scores relative to diploid sample (RNA seq V2 RSEM) was used to find the Pearson's r (correlation coefficient) with cut off value of 1.5. p-value was calculated using t-distribution [39, 40].

Results –

LCN2 levels are increased in colon cancer and lead to an increase in resistance to 5FU. LCN2 mRNA and protein levels were measured by quantitative reverse transcriptase coupled PCR (qRT-PCR) and Western blot analysis, respectively, in eighty matched normal and colon cancer samples collected at the Tata Memorial Centre. LCN2 mRNA and protein levels were substantially elevated in tumor tissues when compared to adjacent morphologically normal tissue (Fig.1A-B). Similarly, LCN2 mRNA expression was elevated in the TCGA colon adenocarcinoma (COAD) dataset (Fig.1C). These results suggest that LCN2 expression is elevated in colon tumor samples.

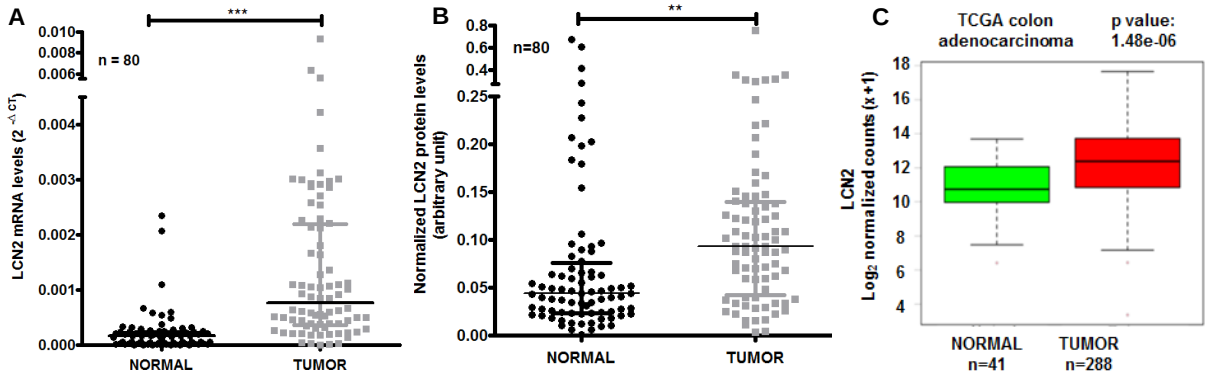

FIGURE 1: LCN2 expression is associated with increased tumor progression and therapy resistance. **A,** mRNA was purified from 80 matched colon tumor and normal paired tissue samples. qRT-PCR reactions for LCN2 were performed and normalized to GAPDH levels and the 2–ΔCT values from normal and tumor samples were plotted. Horizontal bars show the median value of LCN2 levels. **B,** Protein extracts from matched normal and tumor samples were resolved on SDS-PAGE gels and Western blots performed for LCN2. The mean intensity of the LCN2 band was normalized to the total protein levels, as determined by staining the blot with Ponceau-S and the normalized value plotted. Horizontal bars show the median value of intensity. **C,** TCGA data analysis of LCN2 in COAD (TCGA colon cancer) (n = 288) and cut margin samples (n = 41), represented as (log2x + 1). Note that the LCN2 levels are high in the tumor samples as compared to the normal tissue.

Loss of PKP3 in the colon cancer cell line HCT116 led to an increase in LCN2 expression, which was required for tumor progression[34]. In addition to this model (Fig.1D), we generated LCN2 over-expressing lines in HCT116 cells (Fig.1E) and determined secreted LCN2 expression levels in different CRC cell lines (Fig.1F).

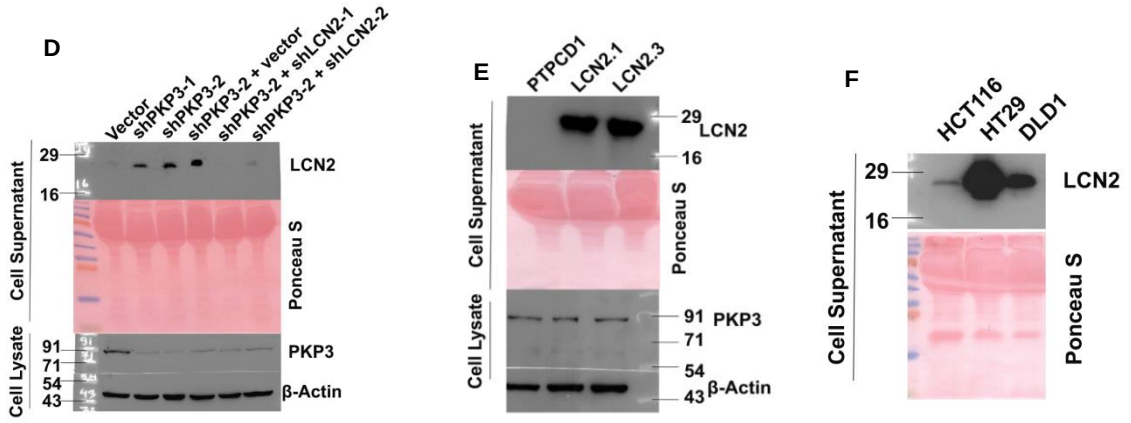

FIGURE 1: Protein extracts prepared from matched tumor and normal tissue samples were resolved on SDS-PAGE gels followed by Western blotting with antibodies to LCN2. The upper panel shows a Ponceau stain of the gel, and the lower panel is the LCN2 Western blot. **(D-E)** 200µg of acetone precipitated cell supernatants, or 100µg of whole cell extracts (WCE) were prepared from HCT116 derived vector control clone (vec), PKP3 knockdown clones (shpkp3-1 and shpkp3-2), the LCN2+PKP3 double knockdown clones (shpkp3-2+shlcn2-1 andshpkp3-2+shlcn2-3) and the shpkp3-2 derived vector control clone (shpkp3-2-vec) **(D)** or the HCT116 derived LCN2 overexpressing clones (LCN2.1 and LCN2.3) and the vector control (PTPCD1) **(E)** or the indicated colon cancer cell lines **(F)** were resolved on SDS PAGE gels followed by Western blotting with the indicated antibodies. A Ponceau-S stain of the blot served as a loading control for LCN2. Western blots for β actin served as a loading control for the WCE.

Overexpression of LCN2 in HCT116 cells led to an increase in colony formation in soft agar (Fig.G) and tumor formation in immunocompromised mice (Fig.H). Similarly, an analysis of the different colon cancer lines demonstrated that increased LCN2 expression correlated with an increase in colony number in soft agar assays (Fig.I).

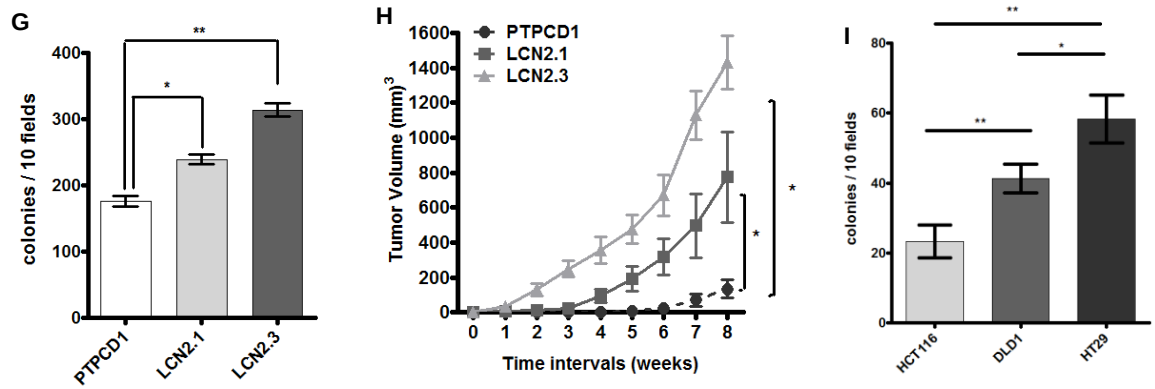

FIGURE 1: **G,** Soft agar colony formation assays were performed with the indicated cell lines. The number of colonies per 10 fields was measured, and the mean and SD are plotted on the Y-axis. **H,** 106 cells of the HCT116 derived LCN2 overexpressing clones LCN2.1 and LCN2.3 or the vector control were injected into immunocompromised mice, and tumor volume was monitored for 8 wk. The mean and SEM is plotted. **I,** Soft

agar colony formation assays were performed with the indicated cell lines. The number of colonies per 10 fields was measured, and the mean and SD are plotted on the Y-axis. Note that increased LCN2 levels correlate with an increase in colony number.

Clonogenic survival assays demonstrated that PKP3 loss led to increased resistance to 5FU (Fig.1J). The observed resistance was dependent on *LCN2* expression as the double knockdown clones showed increased sensitivity to 5FU (Fig.1K). Similar results were observed when the LCN2 over-expressing clones were treated with either 5FU (Fig.1L). Similarly, increased resistance to 5FU correlated with increased LCN2 levels in the different colon cancer cell lines tested (Fig.1M). To determine if the increase in resistance was observed *in vivo*, the vector control or the PKP3 knockdown clones were injected into immunocompromised mice and treated with 5FU when the tumors reached a specific size. The vector control responded to the treatment with 5FU, and tumor size regressed while the PKP3 knockdown clones continued to grow in size (Fig.1N). These results suggest that LCN2 is both necessary and sufficient for the resistance to 5FU.

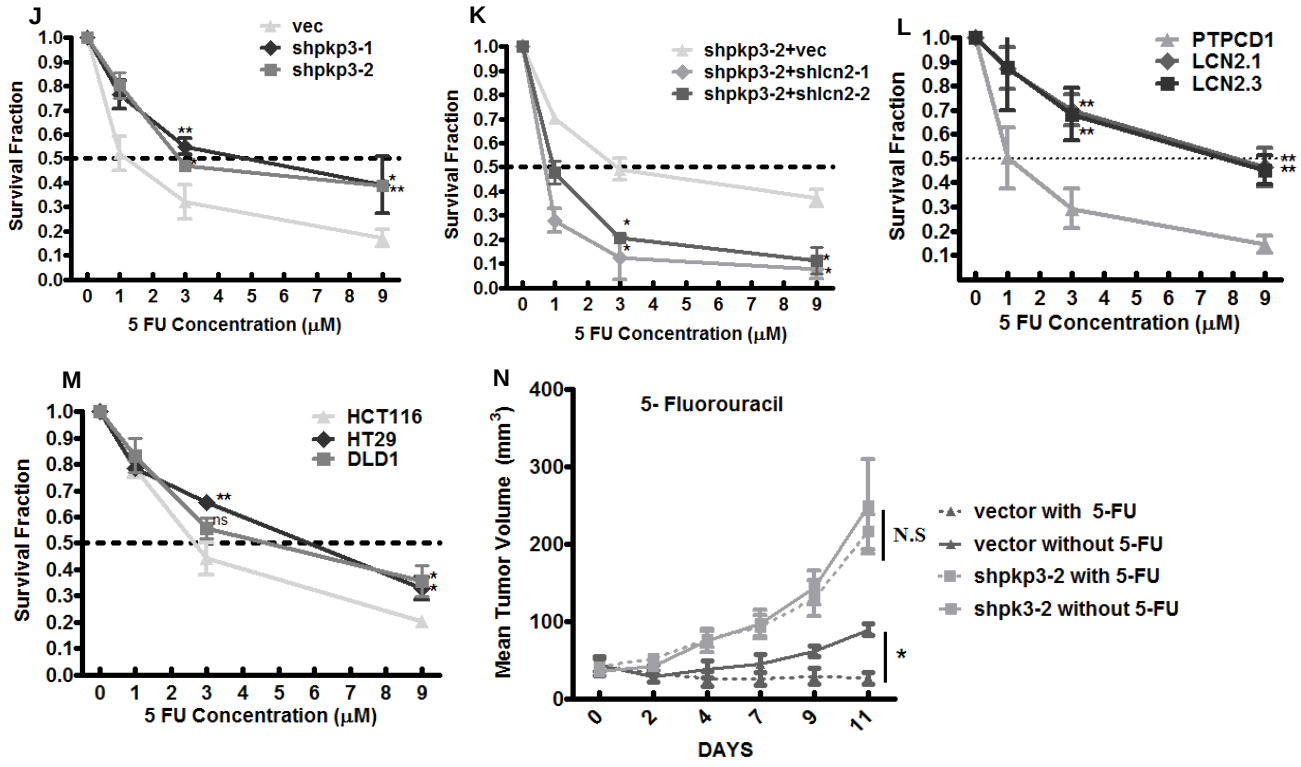

FIGURE 1: **J-M,** the indicated cell lines were treated with different concentrations of 5FU, and clonogenic survival assays were performed. The mean and SD of the survival fraction at different doses of 5FU is plotted. The horizontal line represents the IC50 for each cell line. **N,** Immunocompromised mice were injected subcutaneously in the dorsal flank with $1*10^6$ cells of the HCT116 derived vector control (vec) or PKP3 knockdown clone (shpkp3-2). Once the tumors reached a specific size (30- 50 mm3), mice were either injected with the vehicle control (PBS) or 30 mg/kg 5-FU (IP) thrice a week for 2 wk. Where indicated, the P-value was determined by the student's t-test (***P < .001, **P < .01, *P < .05)

LCN2 expression leads to the clearance of ROS. LCN2 might promote resistance to 5FU by promoting ROS clearance. Cells were untreated or treated with 5FU, and ROS clearance was measured post-treatment in two different assays. While all cells had similar ROS levels at 3 hours post-treatment, the PKP3 knockdown clones showed increased ROS clearance 24 hours post-treatment than the vector controls in both assays (Fig.2A&2D). In contrast, the PKP3 LCN2 double knockdown clones could not clear ROS 24 hours post-treatment (Fig.2A&2D). Similar results were observed with the LCN2 overexpressing clones (Fig.2B&2E) and the different colon cancer cell lines where increased ROS clearance correlated with LCN2 levels (Fig.2C&2F).

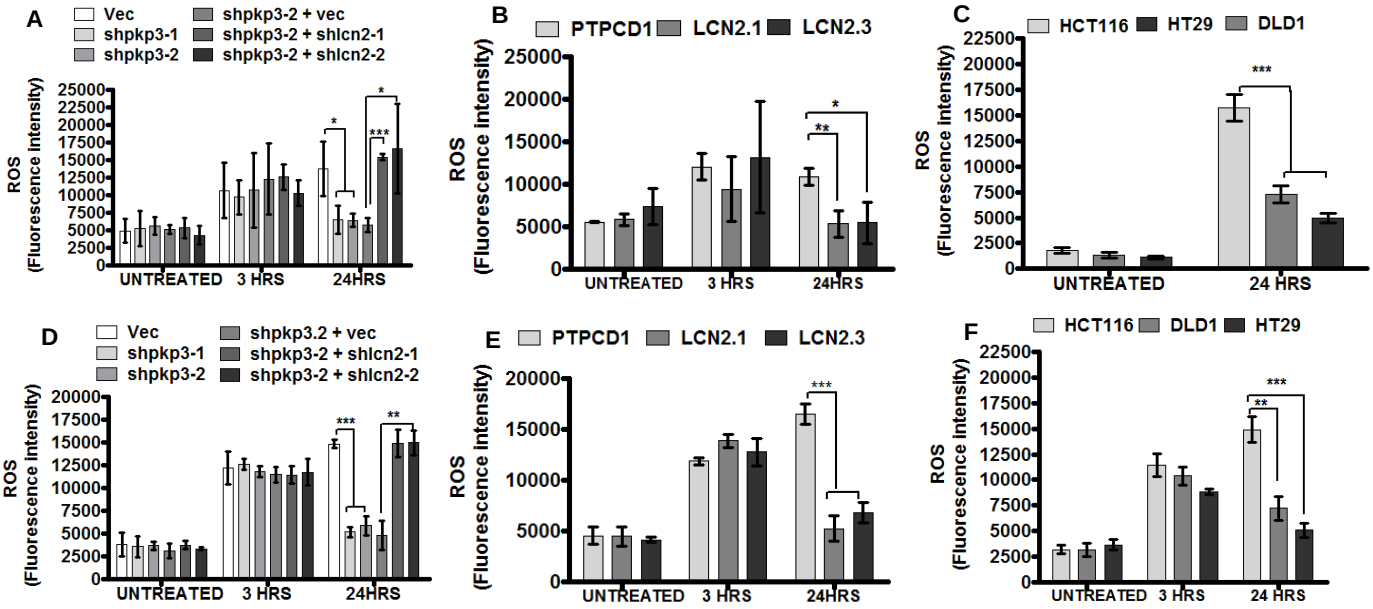

FIGURE 2 LCN2 expression leads to ROS clearance and is dependent on the ability of LCN2 to bind iron. **A-F,** the levels of total ROS were determined using DCFDA **(A-C)** and CellROXTM **(D-F).** The indicated cell lines were incubated in the presence or absence of 5FU for the indicated times, and fluorescence intensity was measured. The mean and SD are plotted on the Y-axis.

The levels of ferrous (Fe^{2+}) and ferric (Fe^{3+}) iron regulate the production of ROS due to a combination of the Haber Weiss reaction and the Fenton reaction[15]. LCN2 binds to Fe^{3+} in the presence of catechol and prevents the conversion of Fe^{3+} to Fe^{2+}, thus breaking the cycle of ROS generation leading to clearance of ROS[41] . Consistent with these observations, the total iron levels were reduced in the PKP3 knockdown cells post-treatment with 5FU compared to the vector control or the PKP3+LCN2 double knockdown cells (Fig 2G). Interestingly, the double knockdown cells had higher intracellular iron levels even in the absence of any treatment. While most of the iron in the untreated cells was ferric iron, this changed upon treatment with 5FU, where the ferrous form was more abundant (Fig.2G). However, the total

iron and ferrous iron levels were much lower in the PKP3 knockdown cells than the vector control and the double knockdown cells. Catechol levels were unchanged in these cells upon treatment with 5FU. Upon treatment with 5FU, the levels of ferrous iron were much lower in the HCT116 derived LCN2 over-expressing cells (Fig.2H) and in the HT29 and DLD1 cells as compared to HCT116, which is consistent with the difference observed in LCN2 levels in these cell lines (Fig.2H&I). Consistent with these results, treating the PKP3 LCN2 double knockdown clones with the iron chelator, deferoxamine (DFO), resulted in increased cell survival upon treatment with 5FU (Fig.2J). To determine if the ability of LCN2 to bind the iron catechol complex was required for the resistance to 5FU, the PKP3+LCN2 double knockdown cells were incubated with recombinant forms of HoloLCN2 (iron-bound), ApoLCN2 (not bound to iron), and an LCN2 mutant (K125AK134A), which cannot bind to the iron catechol complex ([41], before treatment with 5FU. Treatment with the recombinant Holo and Apo LCN2 proteins resulted in increased survival of the double knockdown clones. In contrast, the K125AK134A mutant couldn't confer resistance to 5FU (Fig.2K). These results suggested that the ability of LCN2 to bind the iron–catechol complex is required to stimulate clearance of ROS.

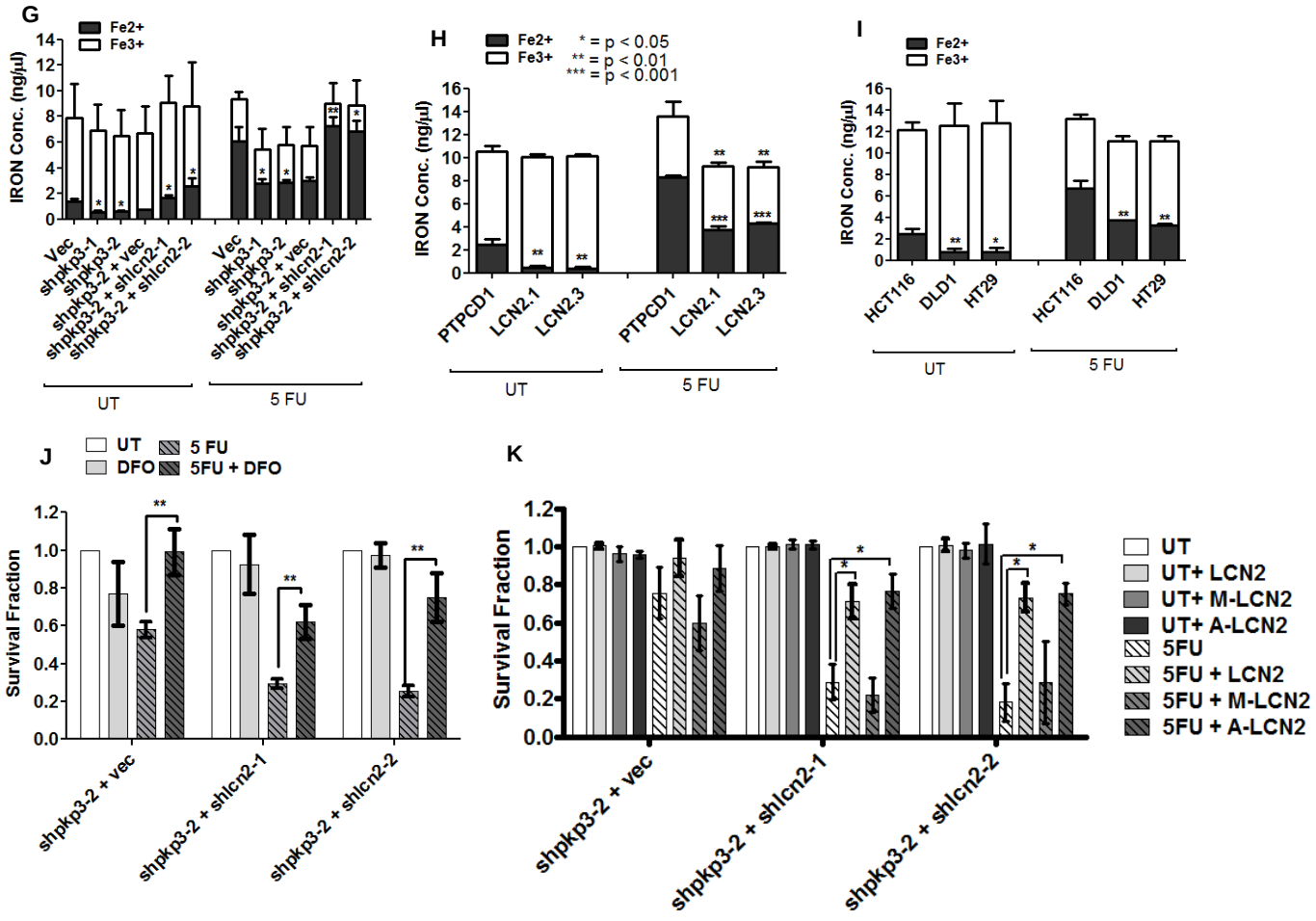

FIGURE 2. G-I, the indicated cell lines were untreated or treated with 5FU for the indicated time points and cellular iron levels measured. The mean and SD are plotted. **J,** the indicated cell lines were treated with the vehicle control or with deferoxamine (DFO), and survival assays were performed. The mean and SD of the survival fraction is plotted on the Y-axis. **K,** the indicated cell lines were seeded and then pre-treated with either the vehicle control, recombinant WT LCN2 (LCN2), ApoLCN2 (A-LCN2), or a mutant LCN2 that does not bind iron (M-LCN2) for 12 h, followed by treatment with 3 μM 5FU for 48 h. The survival fraction is plotted on the Y-axis. The mean and SD is plotted. Where indicated P-values were determined using a student's t test. (*P < .05, **P < .01, ***P < .001 and ns = not significant)

LCN2 inhibits ferroptosis by stimulating GSH production and clearing peroxidated lipids. The results above showed that increased LCN2 expression leads to decreased intracellular levels of ferrous iron. Increased ferrous iron levels are a feature of ferroptosis[4]. Peroxidated lipids accumulate during ferroptosis, and the level of LCN2 expression correlated with the increased clearance of peroxidated lipids upon treatment with 5FU (Fig.3A-C). In contrast, a knockdown of LCN2 in the PKP3 knockdown clones impaired the clearance of peroxidated lipids (Fig.3A). The ability of LCN2 to stimulate the clearance of peroxidated lipids was dependent on the ability of LCN2 to bind the iron-catechol complex as treatment of the PKP3 LCN2 double knockdown clones with recombinant WT LCN2 led to an increased clearance of lipid ROS. In contrast, treatment with the K125AK134A mutant did not restore the ability to clear peroxidated lipids (Fig.3D). These results suggest that the clearance of lipid ROS by LCN2 is dependent on the ability of LCN2 to regulate iron homeostasis.

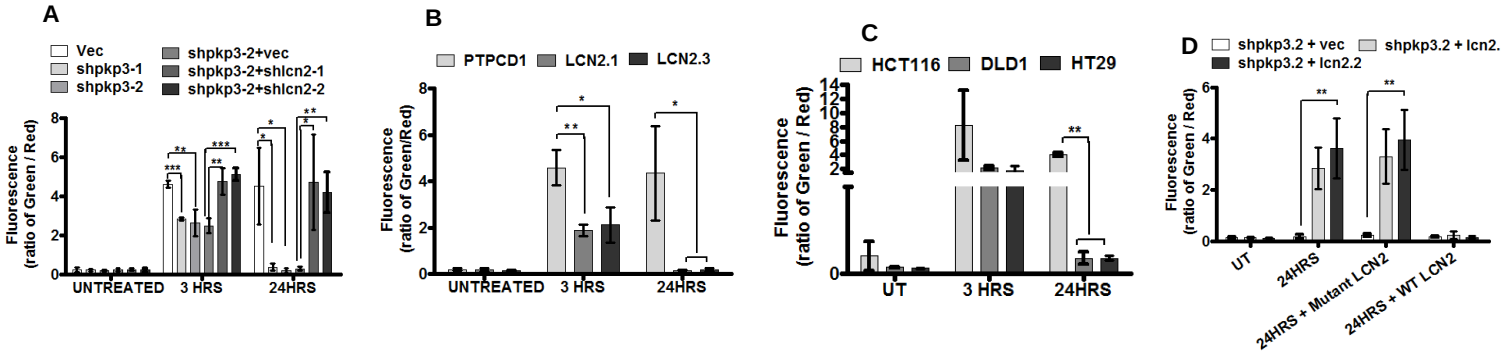

FIGURE 3 LCN2 inhibits ferroptosis by promoting the expression of xCT and GPX4. **A-D,** the indicated cell lines were untreated or treated with 5FU for the indicated time points. The levels of lipid ROS were measured using C11 BODIPY dye (10 μM). The green to red ratio was determined, and the mean and SD are plotted on the Y-axis. Where indicated recombinant WT or mutant LCN2 proteins were added to the media before treatment with 5FU.

The increase in peroxidated lipids is due to a decrease in either the levels of GPX4 or a reduction in intracellular GSH levels due to the inhibition of system x_c^-[4, 5, 7]. We demonstrated that the levels of LCN2 correlated with an increase in the levels of GSH in all the cell lines (Fig.3E-G). Inhibition of LCN2 expression in the PKP3 knockdown clones led to

decreased GSH levels (Fig.3E). To determine if increased GSH levels were due to an increase in the levels of either GPX4 or system x_c^-, we demonstrated that the protein and mRNA levels of the transport subunit of system x_c^-, *xCT* (gene name *SLC7A11*) or *GPX4* were higher in cells with high levels of LCN2 especially post-treatment with 5FU (Fig.3H-K & fig.3L-Q). Though xCT and GPX4 levels increased in all the cell lines upon treatment with 5FU, the increase was more significant in cell lines expressing higher levels of LCN2. In contrast, a knockdown of LCN2 in the PKP3 knockdown cells led to a decrease in xCT levels upon 5FU treatment (Fig.3J & fig.3L&O).

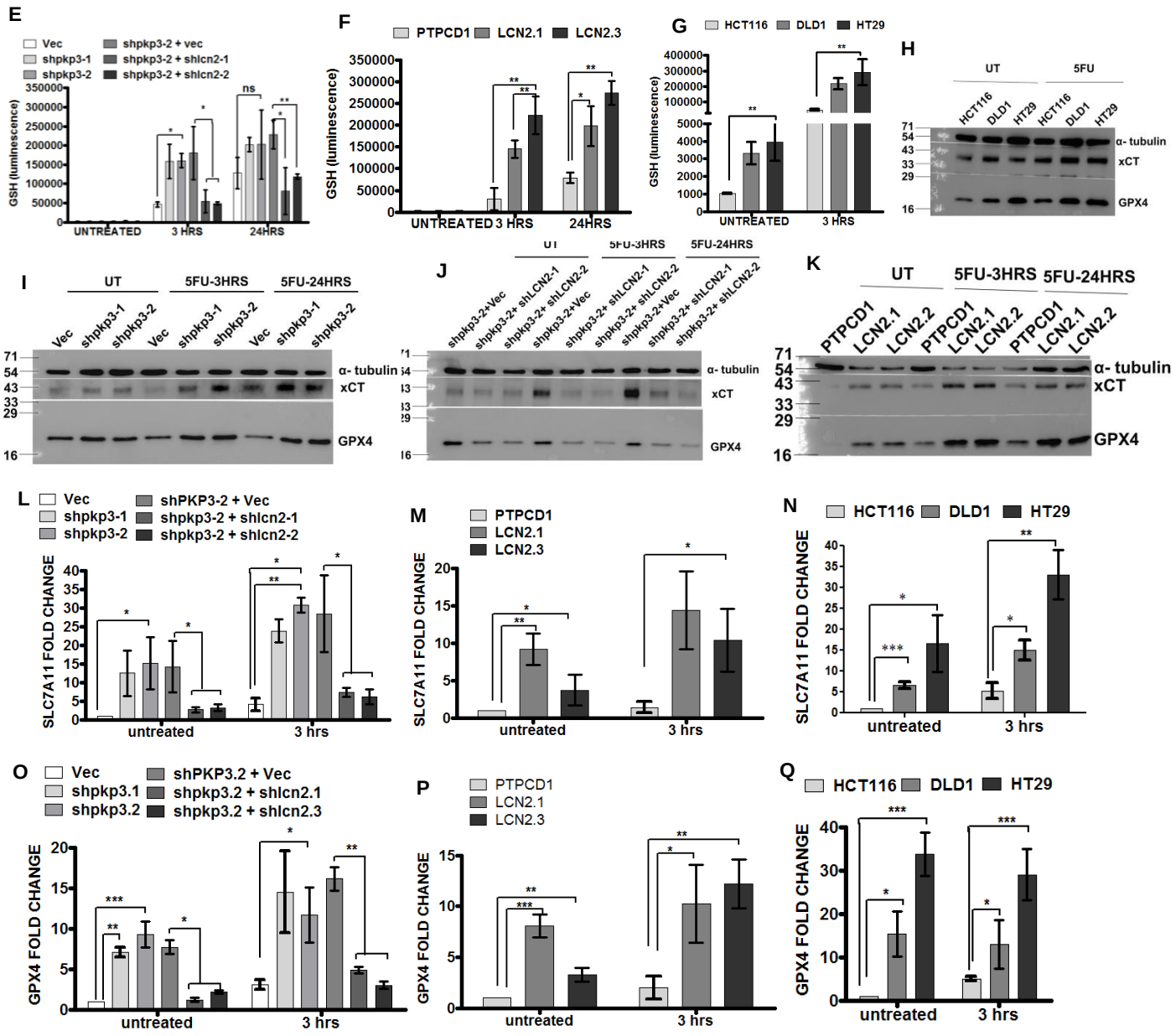

FIGURE 3. E-G, the indicated cell lines were untreated or treated with 5FU for the indicated time points, and GSH levels were determined. The mean fluorescent intensity was determined, and the mean and SD are plotted on the Y-axis. **H-K,** the indicated cell lines were untreated or treated with 5FU for the indicated time points, and protein extracts were prepared as described. 100 μg of protein extracts was resolved on 12% SDS PAGE gels followed by Western blotting with the indicated antibodies. Note that cell lines with elevated LCN2 levels correlated with an increase in xCT and GPX4 levels. α tubulin served as a loading control. L-Q, xCT **(L-N)** and GPX4 **(O-Q)** mRNA levels were determined by qRT-PCR in the indicated cell lines. The fold change was determined, and the mean and SD are plotted on the Y-axis.

Treatment with the ferroptosis inducers, Erastin and RSL-3[7, 10, 11], led to a decrease in survival in cell lines with high levels of LCN2 (Fig.3R). To determine if the reduction in survival in the presence of 5FU had contributions from other cell death pathways, different CRC lines, and PKP3+LCN2 double knockdown clones were treated with the IC_{50} of 5FU in the presence or absence of vehicle control, an apoptosis inhibitor (ZVAD), a necroptosis inhibitor Necrostatin (NEC), a ferroptosis inhibitor ferrostatin (FER) and the cell-permeable cysteine analogue, N-acetyl cysteine (NAC). Treatment with ZVAD or NEC did not significantly increase cell survival in 5FU compared to the vehicle control (Fig.3S-J). In contrast, treatment with either FER or NAC led to a significant increase in survival in the presence of 5FU (Fig.3S-J). Similarly, treatment with the ferroptosis inhibitor Liproxtatin in the presence or absence of 5FU led to increased resistance to 5FU in the LCN2 PKP3 double knockdown clones as compared to the vehicle control (Fig.3K).

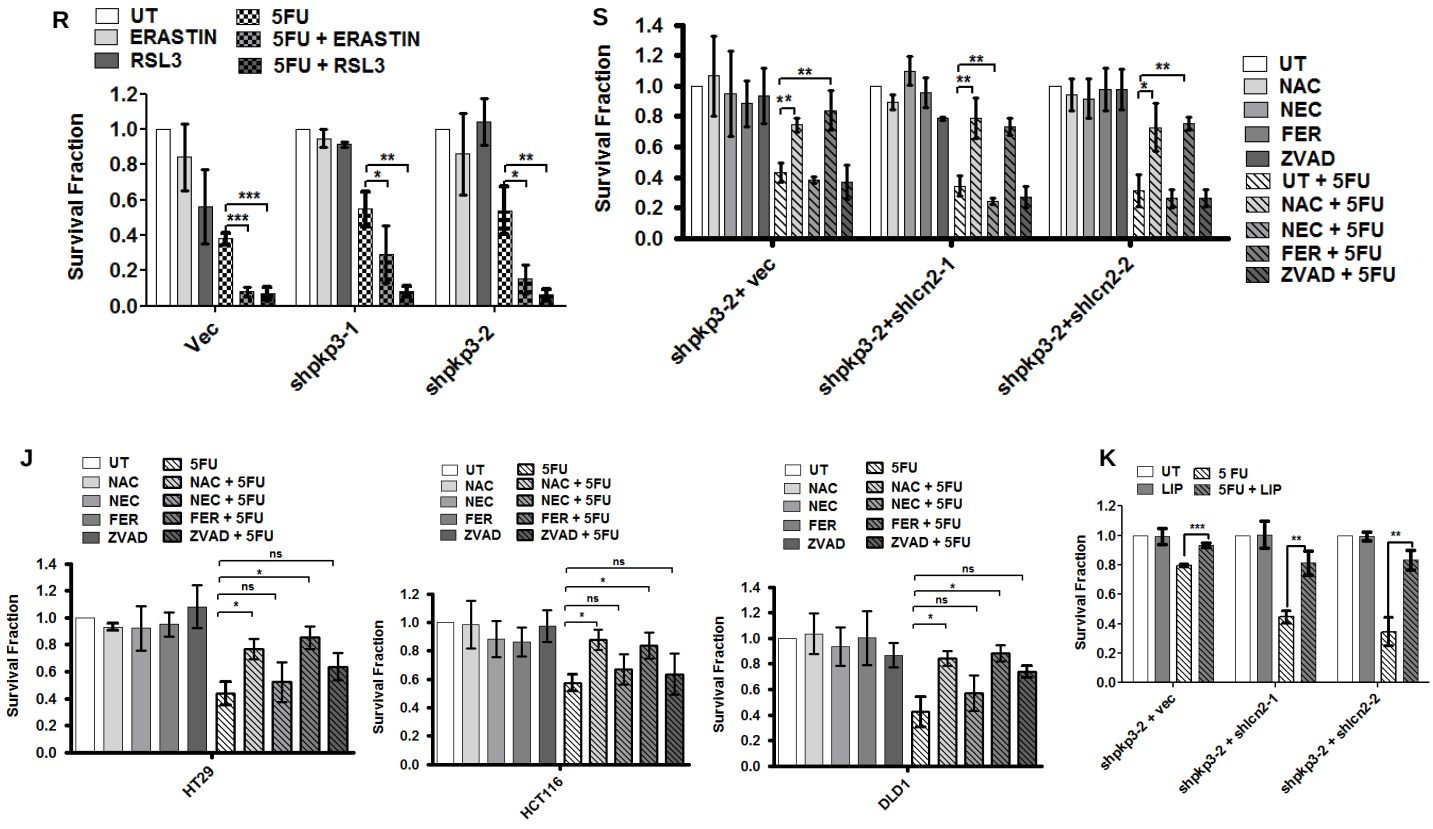

FIGURE 3. **R,** the indicated cell lines were untreated or treated with 5FU in combination with the ferroptosis promoters Erastin or RSL3, and clonogenic survival assays were performed. The mean and SD of three different experiments are plotted**. S,** the indicated cell lines were untreated or treated with 5FU or 5FU in combination with either of N-Acetyl-L-Cysteine (NAC), Necrostatin (NEC), Ferrostatin (FER) and Z-VADFMK (ZVAD), and survival assays were performed. The mean and SD are plotted on the Y-axis. Unless otherwise indicated P-values were obtained using a student's t test (*P < .05, **P < .01, ***P < .001 and ns = not significant. **(J)** The indicated cell lines were untreated or treated with 5FU or 5FU in combination with either of N-Acetyl-L-Cysteine (NAC), Necrostatin (NEC), Ferrostatin (FER), and Z-VADFMK (ZVAD), and survival assays were performed. The mean and standard deviation are plotted on the Y-axis. **(K)** The indicated cell lines were untreated or treated with 5FU in the presence or absence of Liproxtatin, and the survival fraction was determined in three independent experiments. The mean and standard deviation are plotted

xCT expression was inhibited using vector-driven RNAi in cells with high LCN2 levels; the HCT116 derived PKP3 knockdown clones and the colon cancer cell lines, HT29 and DLD1. Stable lines with a knockdown of *xCT* were generated. Loss of *xCT* leads to an increase in the levels of total ROS (Fig.4A-B) and peroxidated lipids (Fig.4C-D) upon treatment with 5FU. *xCT* knockdown also led to a decrease in survival in the presence and absence of 5FU (Fig.4E-F) and reduced colony formation in soft agar (Fig.4G-H). These results suggest that the increase in LCN2 expression leads to an inhibition of ferroptosis induced by 5FU due to alterations in intracellular iron levels and increased system x_c^- activity.

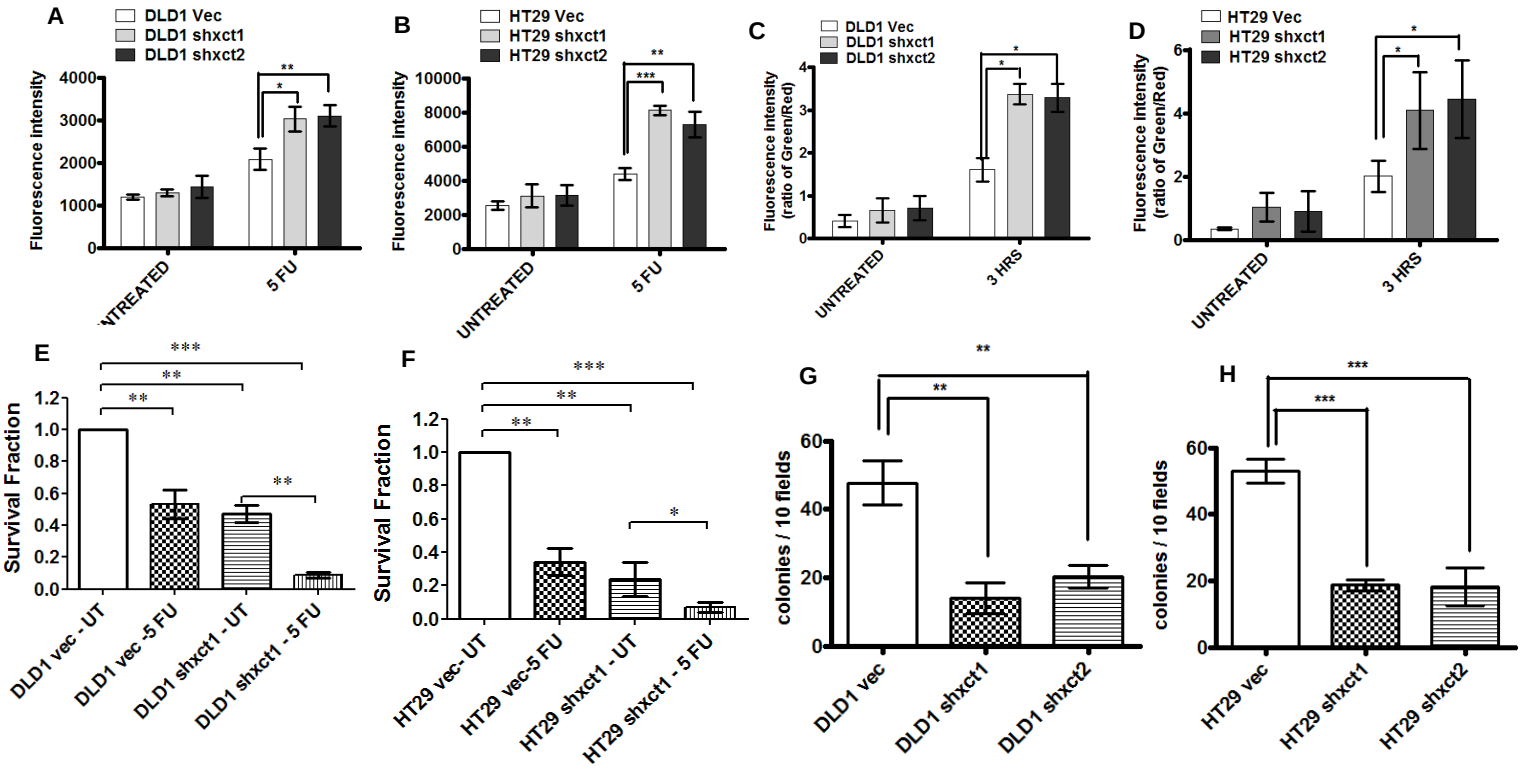

FIGURE 4 Loss of xCT or ETS1 leads to a reversal of therapy resistance in cells expressing LCN2**. A-B**, Stable cell lines expressing the vector control or shRNAs targeting xCT were generated in DLD1 (DLD1+vec, DLD1+shxct1 and DLD1+shxct2) (A) and HT29 (HT29+vec, HT29 +shxct1, HT29+shxct2) **(B)** were untreated or treated with 5FU and ROS levels measured using DCFDA. The mean fluorescent intensity was determined, and the mean and SD plotted on the Y-axis. **C-D**, the levels of lipid ROS were measured using C11 BODIPY dye in the indicated cell lines. The mean and SD of the ratio of green to red fluorescence was plotted on the Y-

axis. **E-F,** the indicated cell lines were untreated or treated with 5FU, and the survival fraction was determined. The mean and SD are plotted. **G-H**, Soft agar assays were performed in the indicated cell lines and the number of colonies per 10 fields determined. The mean and SD are plotted on the Y-axis

LCN2 induces xCT expression by stimulating ETS1 expression. Multiple transcription factors, including *ETS1*, *ATF4*, and *NRF2*, regulate xCT expression [42-44]. An in-silico analysis using JASPAR software identified multiple ETS1 binding sites in the *SLC7A11* promoter (Fig.4I). LCN2 expression led to increased *ETS1* mRNA levels in the HCT116 derived PKP3 knockdown clones and LCN2 over-expressing clones (Fig.4J). LCN2 expression led to increased ETS1 protein levels in all the cell lines tested (Fig.4K-L) in the presence or absence of 5FU.

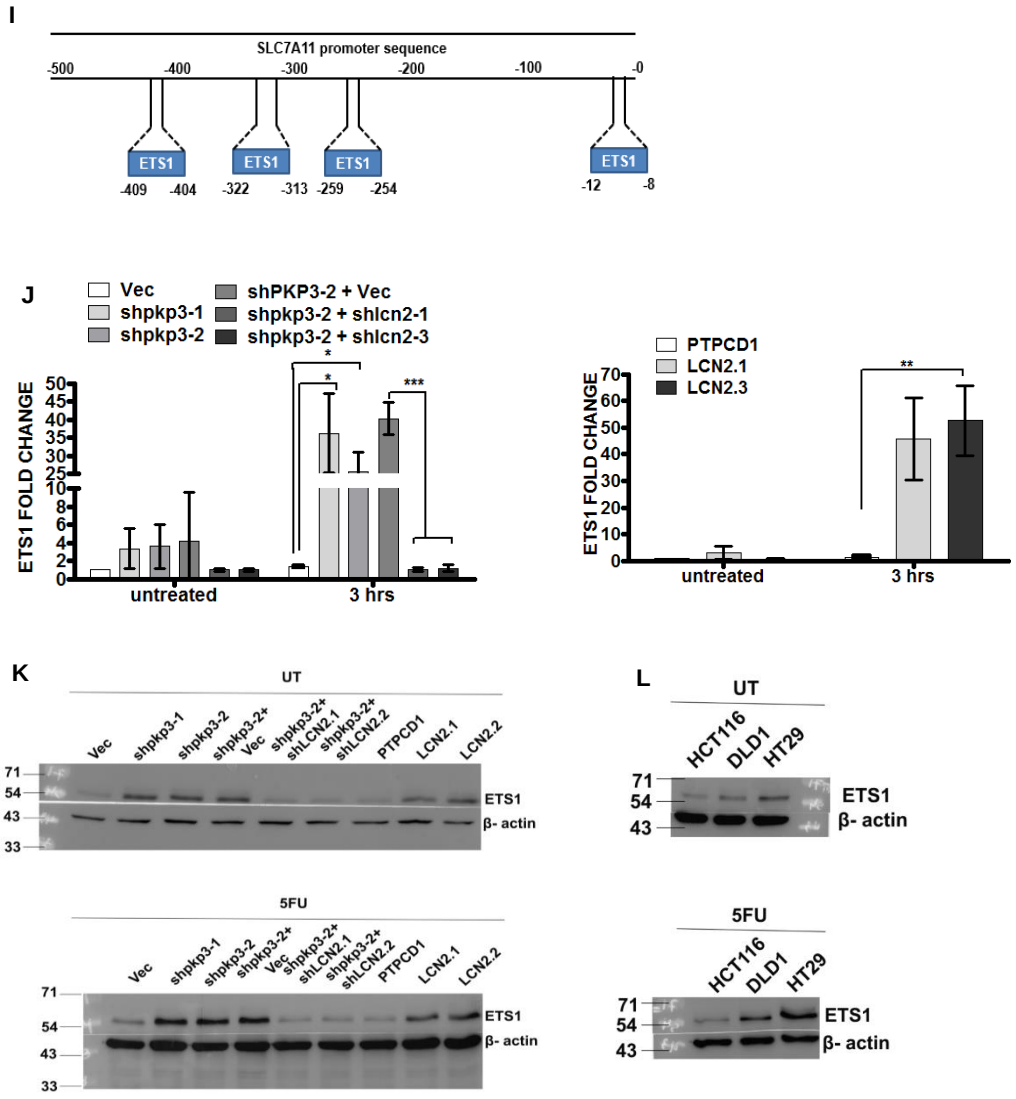

FIGURE 4: A reduction in ETS1 levels leads to a decrease in resistance to 5FU. (I) Diagram of putative ETS1 binding sites in the xCT promoter region obtained using JASPR software. **(J)** The indicated cell lines were untreated or treated with 5FU, and mRNA prepared from the cell lines was used as a template in reverse transcriptase coupled real-time PCR reactions to determine ETS1 levels. The fold change in three independent experiments was measured and the mean and standard deviation plotted on the Y-axis. **K-L** Protein extracts

were prepared from the indicated cell lines that were untreated or treated with 5FU. The extracts were resolved on SDS-PAGE gels followed by Western blots with antibodies to ETS1. Note that ETS1 levels are higher in cells expressing LCN2 and are further stimulated upon 5FU treatment. Western blots for β actin served as a loading control.

Chromatin immunoprecipitation (ChIP) assays followed by real-time PCR demonstrated that ETS1 showed a higher occupancy at the xCT promoter in cell lines with elevated LCN2 levels than the respective vector controls, especially upon treatment with 5FU (Fig.4M-N).

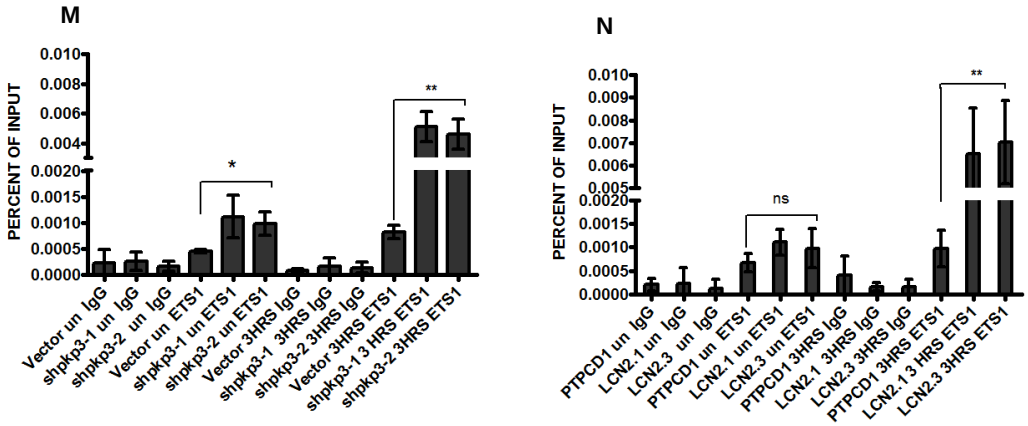

FIGURE 4: **M-N,** ChIP assays were performed using either a non-specific rabbit IgG (IgG) or ETS1 antibodies from the indicated cell lines that were untreated or treated with 5FU, followed by qPCR to detect the xCT promoter. The mean and SD are plotted. Where indicated P-values were determined using a student's t test. (*P < .05, **P < .01, ***P < .001 and ns = not significant)

To further confirm these results, we transiently inhibited *ETS1* expression in the PKP3 knockdown clones and in HT29 cells, both of which have high LCN2 levels (Fig.4O). *xCT* and *GPX4* levels decreased in the ETS1 knockdown clones (Fig.4L). Treatment of these cells with 5FU led to a decrease in survival (Fig.4P), and *LCN2* expression also decreased upon *ETS1* knockdown (Fig.4Q), suggesting the presence of a positive feedback loop between the two genes. CHIP assays demonstrated increased occupancy of the *LCN2* promoter by ETS1 in the presence of 5FU with a smaller but not significant increase in occupancy in the absence of 5FU (Fig.4R). These results suggest that LCN2 stimulates an increase in the transcription factor ETS1, leading to increased xCT expression.

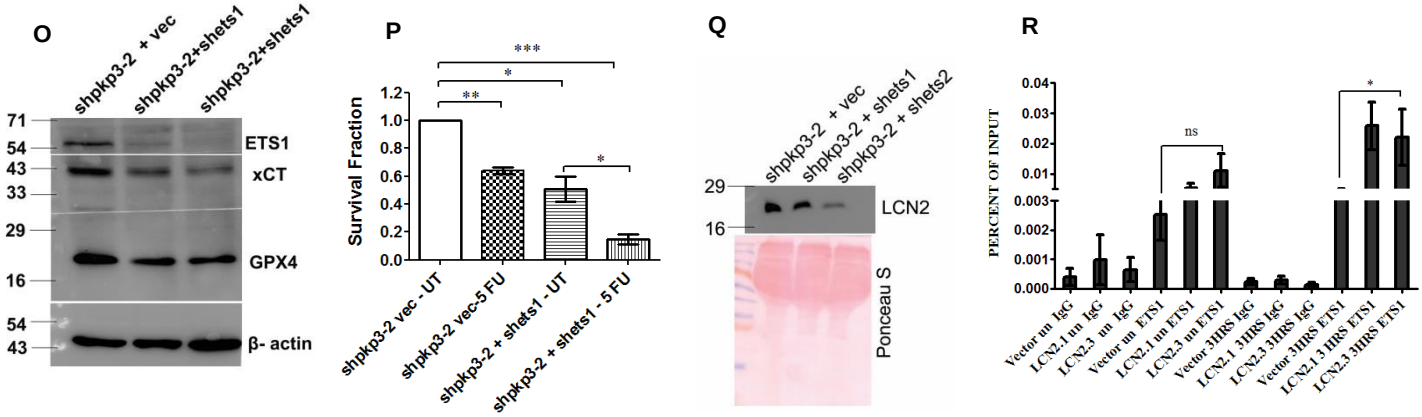

FIGURE 4: **O,** ETS1 expression was inhibited in the indicated cell lines with two different shRNA constructs. Protein extracts were prepared, and 100 µg of the lysates were resolved on 12% SDS PAGE gels followed by Western blotting with antibodies specific to ETS1, xCT and GPX4. Western blots for β actin served as a loading control. The samples for the actin blot were run in a parallel set of lanes on the same gel. Note that a decrease in ETS1 levels leads to a decrease in xCT and GPX4 levels. **P,** ETS1 expression was inhibited in the indicated cell lines with two different shRNA constructs, and survival assays were performed in the presence and absence of 5FU and the survival fraction determined. The mean and SD is plotted. **Q,** 200 µg of acetone precipitated cell supernatants was prepared from the indicated cell lines and resolved on 12% SDS PAGE gels followed by Western blotting with antibodies specific to LCN2. The same blot was stained with Ponceau to serve as a loading control. Note that LCN2 levels are decreased upon a decrease in ETS1 levels. **R,** ChIP assays were performed using either a non-specific rabbit IgG (IgG) or ETS1 antibodies from the indicated cell lines that were untreated or treated with 5FU, followed by qPCR to detect the LCN2 promoter. The mean and SD are plotted. Where indicated P-values were determined using a student's t test. (*P < .05, **P < .01, ***P < .001 and ns = not significant)

Inhibiting LCN2 function leads to sensitivity to 5FU *in vitro* and *in vivo*. We generated a specific monoclonal antibody to LCN2 (3D12B2) and confirmed the specificity by performing Western blots in cells with low and high levels of LCN2 or an LCN2 knockdown (Fig.SF5A-B). The different colon cancer lines were incubated with either the vehicle control, mouse IgG, or 3D12B2 for 12 hours before adding the IC_{50} value of 5FU followed by survival assays. Treatment with the antibody but not mouse IgG or the vehicle control resulted in a significant decrease in survival in response to 5FU treatment (Fig.5A). Similar results were obtained in the HCT116 derived PKP3 knockdown cells (Fig.5B).

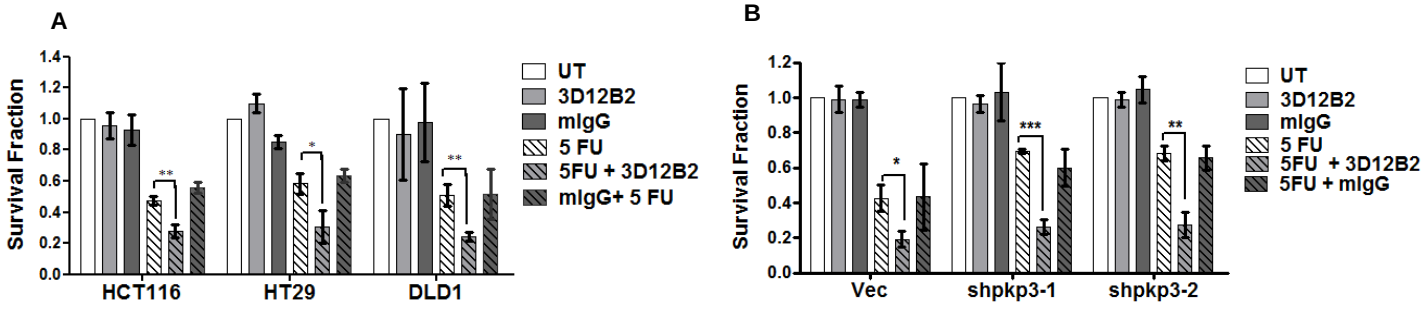

FIGURE 5 Inhibiting LCN2 function inhibits chemoresistance and tumor progression. A-B, the indicated cell lines were treated with 5-FU or the vehicle control in the presence of vehicle control, non-specific mouse IgG (mIgG), or 3D12B2, and survival fractions were determined. The mean and SD are plotted. Note that treatment with 3D12B2 results in an increase in sensitivity to 5FU in LCN2 expressing cells

Treatment with 3D12B2 but not the control antibody led to a decrease in the levels of xCT and GPX4 (Fig.5C), and a decrease in the clearance of peroxidated lipids (Fig.5D).

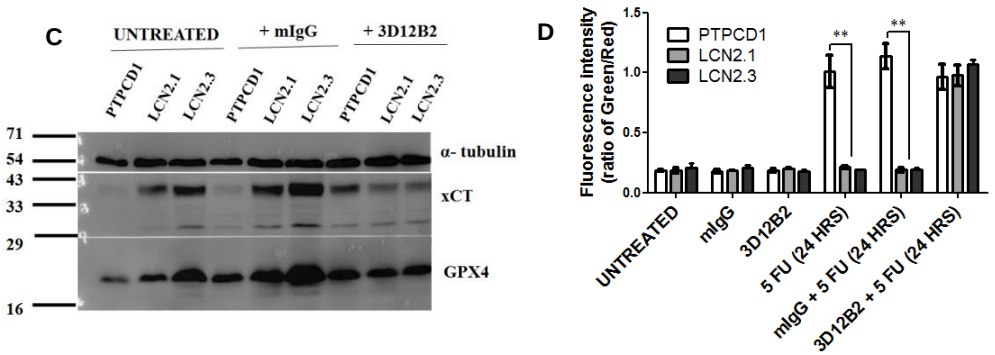

FIGURE 5 C, the indicated cell lines were treated with mIgG or 3D12B2 in the presence or absence of 5FU, and protein extracts resolved on SDS-PAGE gels followed by Western blotting with the indicated antibodies. **D,** the indicated cell lines were treated with 3D12B2 or the vehicle control (PBS) in the presence or absence of 5FU, and the levels of peroxidated lipids were determined. The mean and SD are plotted.

Treatment with 3D12B2 led to an increase in the intracellular levels of ferrous iron, especially upon treatment with 5FU as compared to the vehicle control (Fig.5E). Treatment with 3D12B2 led to decreased colony formation in soft agar compared to treatment with mouse IgG in all cells (Fig.5F-J).

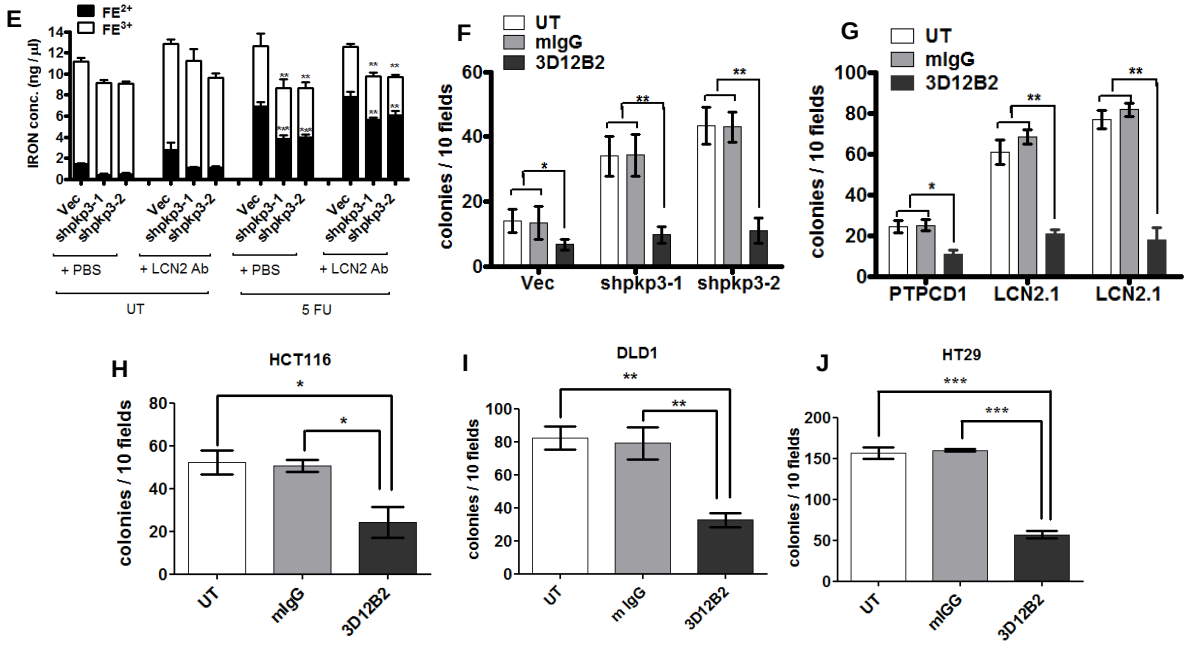

FIGURE 5 E, HCT116 derived vector control and PKP3 knockdown clones were untreated (UT) or pre-treated with 3D12B2 for 12 h, followed by treatment with either the vehicle control or 5FU for 3 h. The cells were harvested, and the levels of total iron, ferric and ferrous iron levels were determined, and the mean and SD plotted on the Y-axis. F-J, Soft agar assays were performed in the indicated cell lines in the presence of the vehicle control (UT), non-specific mouse IgG (mIgG), or 3D12B2, and the number of colonies in 10 low power fields determined in triplicate. The mean and SD were plotted.

Nude mice were injected with the PKP3 knockdown clones or the DLD1 cell line, and once the tumors grew to the appropriate size, they were either untreated or treated with 5-FU as described. In addition to 5-FU treatment, nude mice were also injected with either the vehicle control, non-specific mouse IgG, or 3D12B2, and tumor volume monitored. Tumors formed efficiently in mice injected with the PKP3 knockdown clones or the DLD1 cells in the presence or absence of 5-FU (Fig.5K-L). Treatment with the non-specific mouse IgG did not affect tumor formation. In contrast, treatment with 3D12B2 inhibited tumor progression and induced tumor regression in combination with 5-FU in the PKP3 knockdown clones (Fig.5K). Treatment with 3D12B2 led to a significant decrease in tumor growth in mice injected with the

DLD1 cells, with a further reduction in growth in the presence of 5FU (Fig.5L). These results suggest that 3D12B2 could be a potential molecule for tumor therapy. The different treatments had no significant effects on body weight (Fig.5M-N).

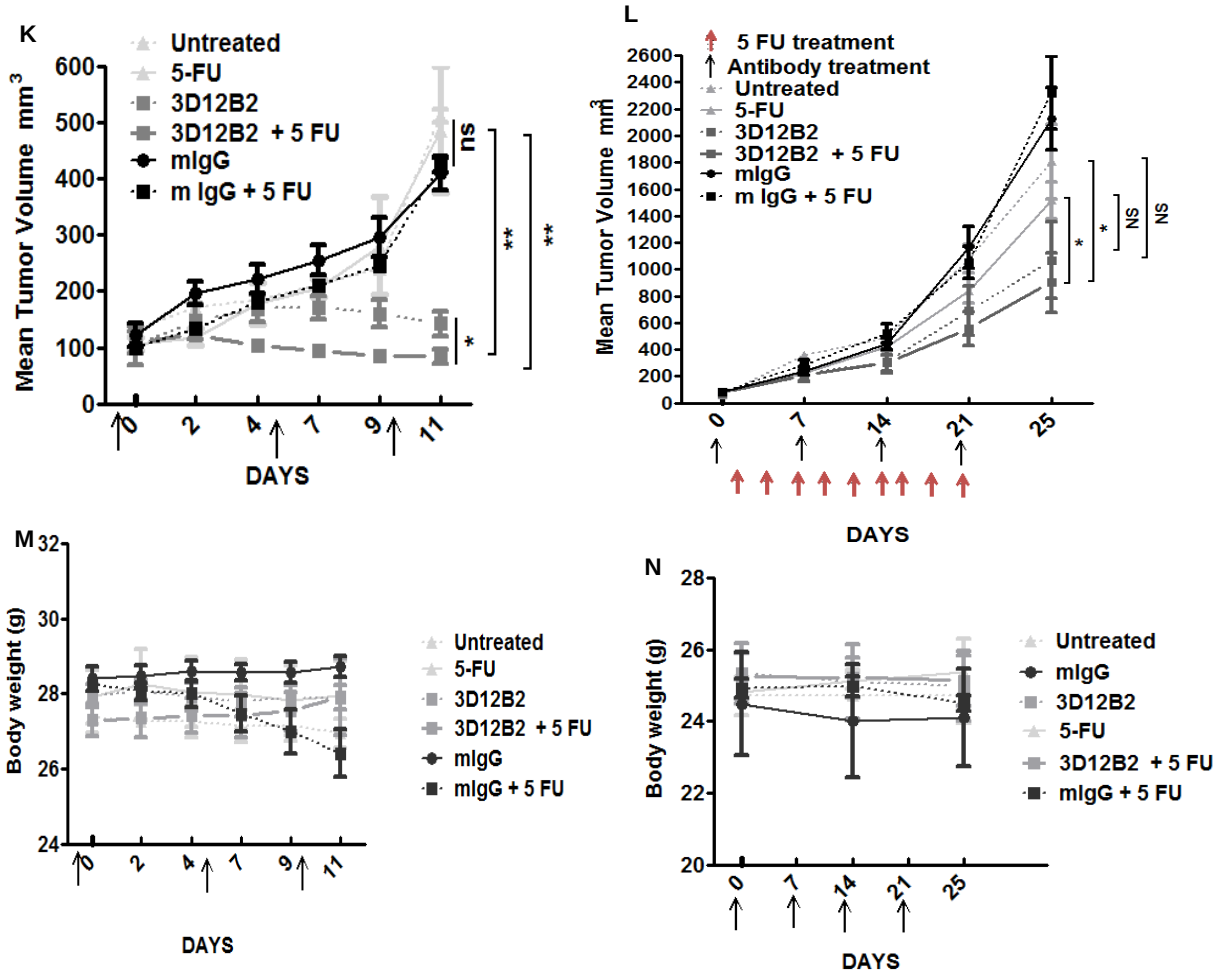

FIGURE 5 K-L, 106 cells of the HCT116 derived PKP3 knockdown clone (shpkp3-2) (K), or a piece of a tumor formed by the DLD1 cell line (L) was injected subcutaneously on the mouse flank. Once the tumors reached a size of 100 mm3, mice were either injected with the vehicle control (PBS) or 30 mg/kg 5-FU (IP) thrice a week for 2 wk. in the presence of either the vehicle control, non-specific mouse IgG (mIgG) or 3D12B2(100 μg IV). The arrows indicate the time of injection. Tumor volume was determined as described. The mean tumor volume and SEM are plotted on the Y-axis. Note that treatment with 3D12B2 results in an inhibition of tumor growth, and treatment with both 3D12B2 and 5FU results in a reduction in tumor growth. **M-N)** The different treatments had no significant effect on body weight. The mean and standard deviation are plotted (n = 5-6 mice per group). Where indicated, P-values were determined using a student's t test (*P < .05, **P < .01, ***P < .001 and ns = not significant).

The results described above suggest that LCN2 inhibits ferroptosis by regulating intracellular iron levels and promoting the expression of *ETS1*, leading to an increase in the levels of *xCT* and *GPX4*. To further extend these studies, we determined *xCT* levels in colon tumor samples

and the adjacent normal tissue. qRT-PCR (Fig.6A) and Western blot analyses (Fig.6B-C) demonstrated that xCT levels were elevated in colon tumor samples as compared to adjacent normal tissue. A positive correlation was observed between the mRNA levels of *LCN2* and *xCT* when analyzing the tumor samples used in this study (Fig.6D).

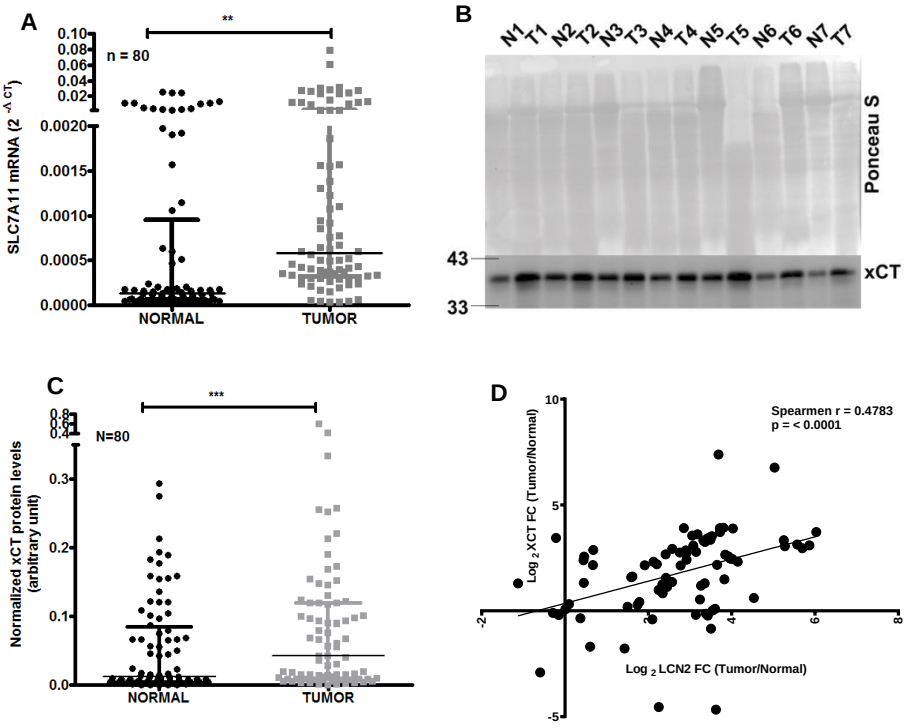

FIGURE 6 LCN2 levels correlate with an increase in xCT levels in human tumor samples. **A,** mRNA was purified from 80 matched colon tumors and normal paired tissue samples. qRT-PCR reactions for xCT were performed and normalized to GAPDH levels and the 2-ΔCT values from normal and tumor samples were plotted. Horizontal bars show the median value of xCT levels. **B-C,** Protein extracts from matched normal and tumor samples were resolved on SDS-PAGE gels and Western blots performed for xCT. The mean intensity of the xCT band was normalized to the total protein levels, as determined by staining the blot with Ponceau-S, and the normalized value plotted. Horizontal bars show the median value of intensity (a.u.). **D,** Pearson's r analysis of SLC7A11 and LCN2. Data represented as scatter plot where r and P correspond to the correlation coefficient and P-value, respectively. Note that there is a positive correlation between LCN2 and SLC7A11 levels.

A larger percentage of stage T3 tumors had higher LCN2 and xCT levels than the adjacent normal (Fig.6E-F). A similar analysis on the COAD cohort from TCGA demonstrated that *xCT* levels were significantly increased in tumor samples compared to normal tissue (Fig.6G).

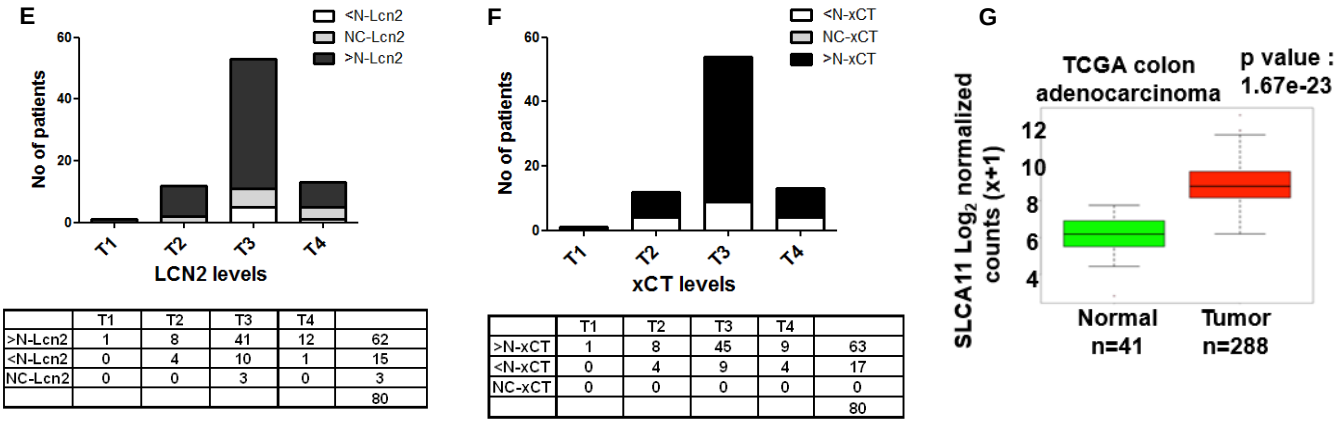

	T1	T2	T3	T4	
>N-Lcn2	1	8	41	12	62
<N-Lcn2	0	4	10	1	15
NC-Lcn2	0	0	3	0	3
					80

	T1	T2	T3	T4	
>N-xCT	1	8	45	9	63
<N-xCT	0	4	9	4	17
NC-xCT	0	0	0	0	0
					80

FIGURE 6: LCN2 and xCT levels are elevated in stage T3 tumors. (E-F) LCN2 **(E)** and xCT **(F)** protein levels were determined by Western blot and their expression as compared to the adjacent normal tissue determined. The number of cases with protein levels less than, equal to or greater than the adjacent normal tissue is plotted on the Y axis and tumor stage on the X axis. Please note that most of the cases in which the LCN2 or xCT levels are greater than the normal tissue is stage T3 tumors. **G,** Boxplot representation of SLC7A11 in COAD (TCGA colon cancer) (n = 288) and cut margin samples (n = 41), represented as (log2x + 1).

A positive correlation was observed between the mRNA levels of *LCN2* and *xCT* in the TCGA cohort (Fig.6H). An analysis of *xCT* levels in the tumor xenografts in immunocompromised mice that were treated with 5FU showed an increase in *xCT* expression in the tumors formed by the *PKP3* knockdown clones than the vector control (Fig.6I). Similarly, *ETS1* mRNA levels significantly increased in colon tumor samples compared to the adjacent normal controls (Fig.6J) and showed a positive correlation with *xCT* levels (Fig. 6K). These results suggest that the pathways underlying the increase in chemoresistance revealed in the cell line data represent what might be happening in human tumor samples.

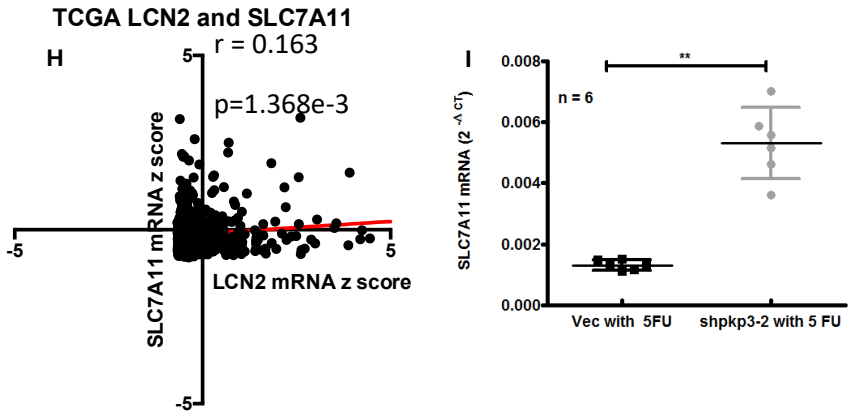

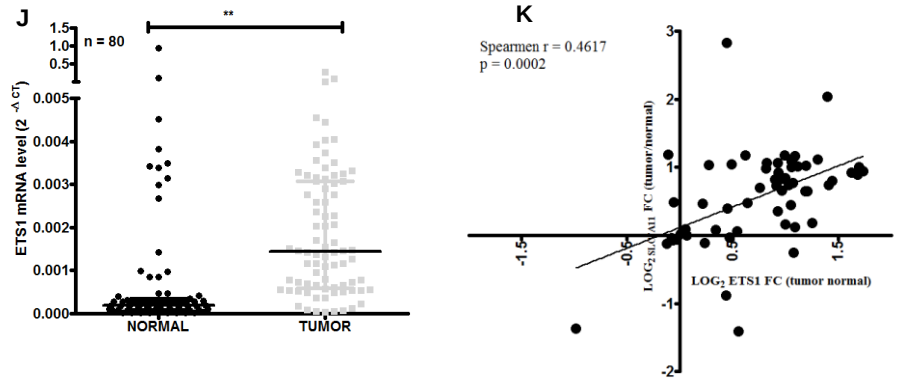

FIGURE 6: H, Pearson's coefficient analysis of SLC7A11 and LCN2 expression in the TCGA data set. The data are represented as a scatter plot where r and p refer to the correlation coefficient and P-value, respectively. Where indicated, P-values were determined using a student's t test. **I**, SLC7A11 mRNA levels were measured in mRNA purified from tumor xenografts. Note that xCT expression is elevated in tumor samples. **J,** mRNA was purified from 80 matched colon tumors and normal paired tissue samples. qRT-PCR reactions for ETS1 were performed and normalized to GAPDH levels and the 2-ΔCT values from normal and tumor samples were plotted. Horizontal bars show the median value of ETS1 levels. **K,** Pearson's r-analysis represented as a scatter plot for SLC7A11 and ETS1 in the tumor samples. r and P represent correlation coefficient and P-value, respectively.

Statistical Analysis –

Data for in vitro experiments is represented as mean and standard deviation (SD) from three independent experiments. For in vivo experiments, it is represented as mean and standard error from the mean (SEM). Statistical significance for adjacent normal and tumor tissue samples (real-time and Western blot quantitation) and in-vivo experiments was calculated using paired t-test. the p-value for TCGA colorectal adenocarcinoma was calculated using Wilcoxon-Mann-Whitney test analysis. Statistical significance for remaining experiments was determined by conducting an unpaired t-test. Data was considered significant for p-value < 0.05. GraphPad (v7) was used to generate the boxplot, bar-graphs, and scatter dot plots.

Discussion –

The results in this report suggest that LCN2 expression leads to tumor progression and chemo-resistance in colon cancer cells., which is consistent with data from human samples, which demonstrate that colon tumor samples have high LCN2 levels as compared to adjacent normal controls as previously reported[45, 46] and there is some evidence that suggests that increased

LCN2 levels are associated with poor survival[47]. LCN2 is an indicator of colon cancer progression from adenoma to carcinoma[20-22], and LCN2 over-expression leads to increased tumor formation in xenograft models of colon cancer[21]. In an APC^{min} mouse model, LCN2 expression inhibits tumor progression in the proximal tissue of the small intestine but is required for tumor progression in the distal region of the small intestine[48]. There is some evidence to suggest that while LCN2 expression is elevated in primary tumors and can lead to tumor progression, LCN2 expression is negatively correlated with metastatic progression in colorectal cancer[49, 50]. Our results demonstrate that LCN2 is required for tumor progression in colon cancer cell lines and is elevated in colon tumor samples, and could be a relevant therapeutic target in colorectal cancer.

LCN2 inhibits ferroptosis by regulating intracellular iron levels and by inducing the expression of *xCT* and *GPX4*. Inhibiting LCN2 function with the anti-LCN2 monoclonal antibody (3D12B2) results in an increase in ferrous iron in cells and a decrease in *GPX4* and *xCT* expression, which promotes ferroptosis, leading to increased sensitivity to chemotherapy and a reduction in tumor formation. Loss of *GPX4* in mice leads to severe toxicity and death of the animal[9], and while a loss of *xCT* is not lethal, it results in defects in spatial working memory[51]. In contrast, the loss of *LCN2* does not result in lethality in mice[52]. Therefore, inhibition of LCN2 function in tumor cells could serve as a novel way of inducing ferroptotic cell death in tumors with minimal toxicity in normal tissues. Thus, LCN2 is a potential drug target in therapy-resistant colorectal cancer and other cancer types[45]. Further, as LCN2 is also over-expressed in other conditions such as age-related macular degeneration[53] and chronic kidney disease[54], the 3D12B2 antibody could also serve as a potential therapeutic in these chronic conditions.

Previous reports suggest that colorectal cancers show an increase in the levels of proteins required for iron import[55]. Excess iron contributes to tumor initiation and progression in humans[56, 57], in human colorectal cancer[58], and mouse models of colon cancer[59]. Increased iron levels lead to ROS generation by iron via the Fenton and Haber-Weiss reactions[60], and tumor progression in the colon is associated with increased ROS levels[61, 62]. In contrast, the results in this report indicate that excessive iron can lead to tumor cell killing through the amplification of ROS production in the context of chemotherapy. A

reduction in intracellular iron levels is observed when LCN2 is over-expressed and is dependent on the ability of LCN2 to bind iron. The ability of LCN2 to bind iron is also required for the ability of LCN2 to inhibit ferroptotic cell death. These results are consistent with the observation that stimulating ferroptosis leads to a reversal of tumor growth and chemo-resistance in multiple tumor types[10-14]. Therefore, the ability to inhibit LCN2 function could be a potential therapeutic strategy for the treatment of multiple tumor types[45].

An increase in intracellular iron levels can stimulate Ferroptosis through the activation of iron transport and a reduction of iron import[63, 64] or the autophagy-mediated degradation of ferritin[65, 66]. This report indicates that LCN2 might be required for the export of iron, thereby leading to chemo-resistance, and is consistent with previous reports suggesting that LCN2 might mediate the export of iron under conditions of iron excess[18]. 3D12B2 might prevent the re-import of LCN2 by blocking the association of LCN2 with the LCN2 receptor, thereby resulting in a decrease in intracellular LCN2 levels leading to a reduction in iron export, consistent with our observations that treatment with 3D12B2 results in an increase in the levels of ferrous iron in cells upon treatment with 5FU. Further, treatment with 3D12B2 results in a decrease in the ability to clear peroxidated lipids, which is consistent with the increase in ferrous iron levels, a hallmark of ferroptosis.

In addition to regulating iron levels, LCN2 inhibits ferroptosis by stimulating the expression of *xCT* and *GPX4* and is observed in the *LCN2* knockdown clones and upon treatment of LCN2 expressing cell lines with 3D12B2. Our data suggest that LCN2 induces the expression of the *ETS1* transcription factor, leading to the expression of *GPX4* and *xCT*, which is consistent with previously published data[43, 67]. While the mechanism underlying the increase in *ETS1* levels upon LCN2 expression is unclear, the stimulation of tyrosine kinase signalling pathways can increase ETS1 expression[68]. LCN2 stimulates the re-localization of EGFR to the membrane in models of chronic kidney disease with a concomitant increase in EGFR activity[54]. Hence, LCN2 might promote *ETS1* expression by stimulating the recycling of receptor tyrosine kinases to the cell surface by inhibiting their degradation in lysosomes[54]. Our observations that loss of either *ETS1* or *xCT* leads to a decrease in cell survival, both in the presence and absence of 5FU, is consistent with the fact that inhibiting LCN2 function *in vivo* leads to decreased tumor formation in the absence of treatment with 5FU, which is probably due to a decrease in *xCT* levels and an increase in the levels of intracellular iron leading to ferroptosis mediated cell death.

The results in this report suggest the following model for LCN2 mediated chemo-resistance (Fig. below). LCN2 inhibits ferroptosis by reducing intracellular iron levels and stimulating the clearance of peroxidated lipids. LCN2 binds iron leading to an inhibition of the conversion of ferric to ferrous iron and promotes iron export. In addition, LCN2 stimulates the expression of *xCT* and *GPX4*, leading to an increase in intracellular glutathione levels and an increased clearance of peroxidated lipids (Fig below). To the best of our knowledge, this is the first example of a gene product that directly impacts both the inhibition of iron accumulation and the reduction of peroxidated lipids. These contribute to the inhibition of ferroptotic cell death and treating these cells with the ferroptosis promoters, Erastin and RSL3, or inhibiting LCN2 function by treating cells with a monoclonal antibody to LCN2 leads to increased ferroptotic cell death. We speculate that the antibody inhibits the association of LCN2 with the LCN2 receptor, thereby decreasing intracellular LCN2 levels leading to an increase in intracellular ferrous iron levels and a decrease in the levels of *GPX4* and *xCT*. These results suggest that the inhibition of LCN2 could be an important therapeutic strategy in multiple tumor types and in tumors that are resistant to conventional chemotherapy.

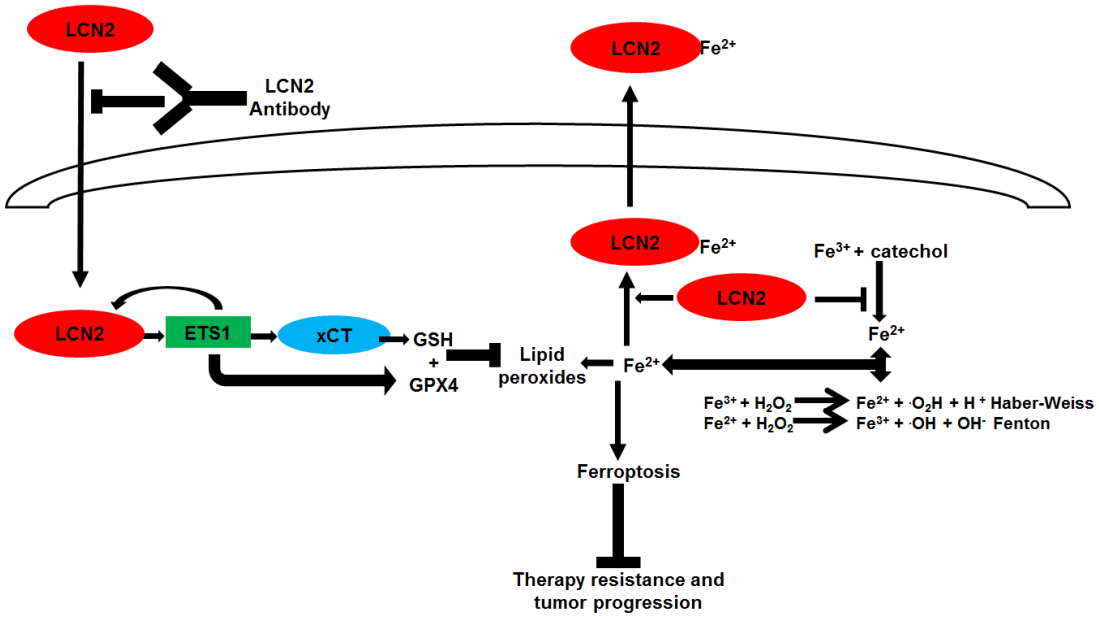

Fig : Model of the mechanism by which LCN2 promotes therapy resistance and tumor progression

Impact of the research in the advancement of knowledge or benefit to mankind –

- **Novelty:** LCN2 is the first example of a gene product that inhibits iron accumulation and promotes the reduction of peroxidated lipids resulting in the inhibition of ferroptosis.
- **Impact:** The LCN2 antibody (3D12B2) could serve as the basis for a potential therapeutic strategy in multiple tumors that exhibit high LCN2 levels and in tumors that are resistant to conventional chemo-radio therapy. It can also be used in other pathogenic conditions driven by high LCN2 levels, such as chronic kidney disease and adult macular degeneration.

Literature references

1. Briffa, R., et al., *Acquired and Intrinsic Resistance to Colorectal Cancer Treatment*, in *Colorectal Cancer - Diagnosis, Screening and Management*, J. Chen, Editor. 2018, Intech Open: London. p. 57-81.
2. Vallam, K.C., et al., *Adenocarcinoma of the Rectum-A Composite of Three Different Subtypes With Varying Outcomes?* Clin Colorectal Cancer, 2016. **15**(2): p. e47-52.
3. Kozovska, Z., V. Gabrisova, and L. Kucerova, *Colon cancer: cancer stem cells markers, drug resistance and treatment.* Biomed Pharmacother, 2014. **68**(8): p. 911-6.
4. Dixon, S.J. and B.R. Stockwell, *The Hallmarks of Ferroptosis.* Annual Review of Cancer Biology, 2019. **3**: p. 35-54.
5. Dixon, S.J., et al., *Ferroptosis: an iron-dependent form of nonapoptotic cell death.* Cell, 2012. **149**(5): p. 1060-72.
6. Yang, W.S., et al., *Peroxidation of polyunsaturated fatty acids by lipoxygenases drives ferroptosis.* Proc Natl Acad Sci U S A, 2016. **113**(34): p. E4966-75.
7. Yang, W.S., et al., *Regulation of ferroptotic cancer cell death by GPX4.* Cell, 2014. **156**(1-2): p. 317-331.
8. Dixon, S.J., et al., *Pharmacological inhibition of cystine-glutamate exchange induces endoplasmic reticulum stress and ferroptosis.* Elife, 2014. **3**: p. e02523.
9. Friedmann Angeli, J.P., et al., *Inactivation of the ferroptosis regulator Gpx4 triggers acute renal failure in mice.* Nat Cell Biol, 2014. **16**(12): p. 1180-91.
10. Dolma, S., et al., *Identification of genotype-selective antitumor agents using synthetic lethal chemical screening in engineered human tumor cells.* Cancer Cell, 2003. **3**(3): p. 285-96.
11. Yagoda, N., et al., *RAS-RAF-MEK-dependent oxidative cell death involving voltage-dependent anion channels.* Nature, 2007. **447**(7146): p. 864-8.
12. Yang, W.S. and B.R. Stockwell, *Synthetic lethal screening identifies compounds activating iron-dependent, nonapoptotic cell death in oncogenic-RAS-harboring cancer cells.* Chem Biol, 2008. **15**(3): p. 234-45.
13. Hangauer, M.J., et al., *Drug-tolerant persister cancer cells are vulnerable to GPX4 inhibition.* Nature, 2017. **551**(7679): p. 247-250.
14. Viswanathan, V.S., et al., *Dependency of a therapy-resistant state of cancer cells on a lipid peroxidase pathway.* Nature, 2017. **547**(7664): p. 453-457.
15. Chakraborty, S., et al., *The multifaceted roles of neutrophil gelatinase associated lipocalin (NGAL) in inflammation and cancer.* Biochim Biophys Acta, 2012. **1826**(1): p. 129-69.

16. Schmidt-Ott, K.M., et al., *Neutrophil gelatinase-associated lipocalin-mediated iron traffic in kidney epithelia.* Curr Opin Nephrol Hypertens, 2006. **15**(4): p. 442-9.
17. Playford, R.J., et al., *Effects of mouse and human lipocalin homologues 24p3/lcn2 and neutrophil gelatinase-associated lipocalin on gastrointestinal mucosal integrity and repair.* Gastroenterology, 2006. **131**(3): p. 809-17.
18. Devireddy, L.R., et al., *A cell-surface receptor for lipocalin 24p3 selectively mediates apoptosis and iron uptake.* Cell, 2005. **123**(7): p. 1293-305.
19. Rodvold, J.J., N.R. Mahadevan, and M. Zanetti, *Lipocalin 2 in cancer: when good immunity goes bad.* Cancer Lett, 2012. **316**(2): p. 132-8.
20. Nielsen, B.S., et al., *Induction of NGAL synthesis in epithelial cells of human colorectal neoplasia and inflammatory bowel diseases.* Gut, 1996. **38**(3): p. 414-20.
21. Sun, Y., et al., *NGAL expression is elevated in both colorectal adenoma-carcinoma sequence and cancer progression and enhances tumorigenesis in xenograft mouse models.* Clin Cancer Res, 2011. **17**(13): p. 4331-40.
22. McLean, M.H., et al., *Expression of neutrophil gelatinase-associated lipocalin in colorectal neoplastic progression: a marker of malignant potential?* Br J Cancer, 2013. **108**(12): p. 2537-41.
23. Tsutomu Miyamoto*, H.K., Yasushi Yamada, Hisanori Kobara,, H.A. Ryoichi Asaka, Shotaro Higuchi, Koichi Ida, David Hamisi Mvunta,, and T. Shiozawa, *Lipocalin 2 Enhances Migration and Resistance against Cisplatin in Endometrial Carcinoma Cells.* PLOS ONE, 2016. **11**(5): p. p e0155220.
24. Masashi Shiiba, K.S., KAZUAKI FUSHIMI1, TAKASHI ISHIGAMI1, KEIJI SHINOZUKA1,, Y.K. DAI NAKASHIMA1, HIROFUMI KOIKE1, ATSUSHI KASAMATSU1, YOSUKE SAKAMOTO1,, and K.U. KATSUNORI OGAWARA1, YUICHI TAKIGUCHI2 and HIDEKI TANZAWA1, *Lipocalin-2 is associated with radioresistancein oral cancer and lung cancer cells.* INTERNATIONAL JOURNAL OF ONCOLOGY, 2012. **42**: p. 1197-1204.
25. Bauer, M., et al., *Neutrophil gelatinase-associated lipocalin (NGAL) is a predictor of poor prognosis in human primary breast cancer.* Breast Cancer Res Treat, 2008. **108**(3): p. 389-97.
26. Stoesz, S.P., et al., *Heterogeneous expression of the lipocalin NGAL in primary breast cancers.* Int J Cancer, 1998. **79**(6): p. 565-72.
27. Yang, J., et al., *Lipocalin 2 promotes breast cancer progression.* Proc Natl Acad Sci U S A, 2009. **106**(10): p. 3913-8.
28. Berger, T., et al., *Disruption of the Lcn2 gene in mice suppresses primary mammary tumor formation but does not decrease lung metastasis.* Proc Natl Acad Sci U S A, 2010. **107**(7): p. 2995-3000.
29. Leng, X., et al., *Inhibition of lipocalin 2 impairs breast tumorigenesis and metastasis.* Cancer Res, 2009. **69**(22): p. 8579-84.
30. Guo, P., et al., *ICAM-1-Targeted, Lcn2 siRNA-Encapsulating Liposomes are Potent Anti-angiogenic Agents for Triple Negative Breast Cancer.* Theranostics, 2016. **6**(1): p. 1-13.
31. Guo, P., et al., *Inhibiting metastatic breast cancer cell migration via the synergy of targeted, pH-triggered siRNA delivery and chemokine axis blockade.* Mol Pharm, 2014. **11**(3): p. 755-65.
32. Tong, Z., et al., *Neutrophil gelatinase-associated lipocalin: a novel suppressor of invasion and angiogenesis in pancreatic cancer.* Cancer Res, 2008. **68**(15): p. 6100-8.
33. Yang, J., et al., *Lipocalin 2 is a novel regulator of angiogenesis in human breast cancer.* FASEB J, 2013. **27**(1): p. 45-50.
34. Basu, S., et al., *Plakophilin3 loss leads to an increase in lipocalin2 expression, which is required for tumour formation.* Exp Cell Res, 2018. **369**: p. 251-65.
35. Kundu, S.T., et al., *Plakophilin3 downregulation leads to a decrease in cell adhesion and promotes metastasis.* Int J Cancer, 2008. **123**(10): p. 2303-2314.

36. Mir, R., et al., *Wnt/beta-catenin signaling regulated SATB1 promotes colorectal cancer tumorigenesis and progression.* Oncogene, 2016. **35**(13): p. 1679-91.
37. Dalal, S.N., et al., *Cytoplasmic localization of human cdc25C during interphase requires an intact 14-3-3 binding site.* Mol Cell Biol, 1999. **19**(6): p. 4465-79.
38. Basu, S., R. Thorat, and S.N. Dalal, *MMP7 is required to mediate cell invasion and tumor formation upon Plakophilin3 loss.* PLoS One, 2015. **10**(4): p. e0123979.
39. Cerami, E., et al., *The cBio cancer genomics portal: an open platform for exploring multidimensional cancer genomics data.* Cancer Discov, 2012. **2**(5): p. 401-4.
40. Gao, J., et al., *Integrative analysis of complex cancer genomics and clinical profiles using the cBioPortal.* Sci Signal, 2013. **6**(269): p. pl1.
41. Bao, G., et al., *Iron traffics in circulation bound to a siderocalin (Ngal)-catechol complex.* Nat Chem Biol, 2010. **6**(8): p. 602-9.
42. Habib, E., et al., *Expression of xCT and activity of system xc(-) are regulated by NRF2 in human breast cancer cells in response to oxidative stress.* Redox Biol, 2015. **5**: p. 33-42.
43. Lim, J.K.M., et al., *Cystine/glutamate antiporter xCT (SLC7A11) facilitates oncogenic RAS transformation by preserving intracellular redox balance.* Proc Natl Acad Sci U S A, 2019. **116**(19): p. 9433-9442.
44. Ye, P., et al., *Nrf2- and ATF4-dependent upregulation of xCT modulates the sensitivity of T24 bladder carcinoma cells to proteasome inhibition.* Mol Cell Biol, 2014. **34**(18): p. 3421-34.
45. Candido, S., et al., *Roles of neutrophil gelatinase-associated lipocalin (NGAL) in human cancer.* Oncotarget, 2014. **5**(6): p. 1576-94.
46. Santiago-Sanchez, G.S., et al., *Biological Functions and Therapeutic Potential of Lipocalin 2 in Cancer.* Int J Mol Sci, 2020. **21**(12).
47. Maier, H.T., et al., *Up-regulation of neutrophil gelatinase-associated lipocalin in colorectal cancer predicts poor patient survival.* World J Surg, 2014. **38**(8): p. 2160-7.
48. Reilly, P.T., et al., *Lipocalin 2 performs contrasting, location-dependent roles in APCmin tumor initiation and progression.* Oncogene, 2013. **32**(10): p. 1233-9.
49. Kim, S.L., et al., *Lipocalin 2 negatively regulates cell proliferation and epithelial to mesenchymal transition through changing metabolic gene expression in colorectal cancer.* Cancer Sci, 2017. **108**(11): p. 2176-2186.
50. Lee, H.J., et al., *Ectopic expression of neutrophil gelatinase-associated lipocalin suppresses the invasion and liver metastasis of colon cancer cells.* Int J Cancer, 2006. **118**(10): p. 2490-7.
51. De Bundel, D., et al., *Loss of system x(c)- does not induce oxidative stress but decreases extracellular glutamate in hippocampus and influences spatial working memory and limbic seizure susceptibility.* J Neurosci, 2011. **31**(15): p. 5792-803.
52. Flo, T.H., et al., *Lipocalin 2 mediates an innate immune response to bacterial infection by sequestrating iron.* Nature, 2004. **432**(7019): p. 917-21.
53. Ghosh, S., et al., *Neutrophils homing into the retina trigger pathology in early age-related macular degeneration.* Commun Biol, 2019. **2**: p. 348.
54. Yammine, L., et al., *Lipocalin-2 Regulates Epidermal Growth Factor Receptor Intracellular Trafficking.* Cell Rep, 2019. **29**(7): p. 2067-2077 e6.
55. Brookes, M.J., et al., *Modulation of iron transport proteins in human colorectal carcinogenesis.* Gut, 2006. **55**(10): p. 1449-60.
56. Torti, S.V. and F.M. Torti, *Iron and cancer: more ore to be mined.* Nat Rev Cancer, 2013. **13**(5): p. 342-55.
57. Torti, S.V. and F.M. Torti, *Iron: The cancer connection.* Mol Aspects Med, 2020: p. 100860.
58. Nelson, R.L., *Iron and colorectal cancer risk: human studies.* Nutr Rev, 2001. **59**(5): p. 140-8.
59. Radulescu, S., et al., *Luminal iron levels govern intestinal tumorigenesis after Apc loss in vivo.* Cell Rep, 2012. **2**(2): p. 270-82.
60. Toyokuni, S., *Iron-induced carcinogenesis: the role of redox regulation.* Free Radic Biol Med, 1996. **20**(4): p. 553-66.

61. Myant, K.B., et al., *ROS production and NF-kappaB activation triggered by RAC1 facilitate WNT-driven intestinal stem cell proliferation and colorectal cancer initiation.* Cell Stem Cell, 2013. **12**(6): p. 761-73.
62. Wang, C., et al., *Cholesterol Enhances Colorectal Cancer Progression via ROS Elevation and MAPK Signaling Pathway Activation.* Cell Physiol Biochem, 2017. **42**(2): p. 729-742.
63. Gao, M., et al., *Glutaminolysis and Transferrin Regulate Ferroptosis.* Mol Cell, 2015. **59**(2): p. 298-308.
64. Ma, S., et al., *Ferroptosis is induced following siramesine and lapatinib treatment of breast cancer cells.* Cell Death Dis, 2016. **7**: p. e2307.
65. Gao, M., et al., *Ferroptosis is an autophagic cell death process.* Cell Res, 2016. **26**(9): p. 1021-32.
66. Hou, W., et al., *Autophagy promotes ferroptosis by degradation of ferritin.* Autophagy, 2016. **12**(8): p. 1425-8.
67. Verschoor, M.L. and G. Singh, *Ets-1 regulates intracellular glutathione levels: key target for resistant ovarian cancer.* Mol Cancer, 2013. **12**(1): p. 138.
68. Dittmer, J., *The biology of the Ets1 proto-oncogene.* Mol Cancer, 2003. **2**: p. 29.